Water Resources Research

RESEARCH ARTICLE
10.1029/2018WR023527

Dynamics of Surface-Water Connectivity in a Low-Gradient Meandering River Floodplain

Jonathan A. Czuba[1], Scott R. David[2], Douglas A. Edmonds[2], and Adam S. Ward[3]

[1]Department of Biological Systems Engineering and the Global Change Center, Virginia Tech, Blacksburg, VA, USA, [2]Department of Earth and Atmospheric Sciences, Indiana University Bloomington, Bloomington, IN, USA, [3]School of Public and Environmental Affairs, Indiana University Bloomington, Bloomington, IN, USA

Key Points:
- Floodplain inundation occurs roughly 19 days per year, which obfuscates the notion of bankfull flow
- Highly connected, meandering river-floodplain systems have three flow-dependent regimes: single thread, multithread, and fully inundated
- We quantify the surface-water connectivity of a river-floodplain system with metrics of residence time and river-floodplain exchange

Supporting Information:
- Supporting Information S1

Correspondence to:
J. A. Czuba,
jczuba@vt.edu

Citation:
Czuba, J. A., David, S. R., Edmonds, D. A., & Ward, A. S. (2019). Dynamics of surface-water connectivity in a low-gradient meandering river floodplain. *Water Resources Research*, *55*, 1849–1870. https://doi.org/10.1029/2018WR023527

Received 18 JUN 2018
Accepted 14 JAN 2019
Accepted article online 22 JAN 2019
Published online 4 MAR 2019
Corrected 22 MAY 2019

This article was corrected on 22 MAY 2019. See the end of the full text for details

Abstract High-resolution topography reveals that floodplains along meandering rivers in Indiana commonly contain intermittently flowing channel networks. We investigated how the presence of floodplain channels affects lateral surface-water connectivity between a river and floodplain (specifically exchange flux and timescales of transport) as a function of flow stage in a low-gradient river-floodplain system. We constructed a two-dimensional, surface-water hydrodynamic model using Hydrologic Engineering Center's River Analysis System (HEC-RAS) 2D along 32 km of floodplain (56 km along the river) of the East Fork White River near Seymour, Indiana, USA, using lidar elevation data and surveyed river bathymetry. The model was calibrated using land-cover specific roughness to elevation-discharge data from a U.S. Geological Survey gage and validated against high-water marks, an aerial photo showing the spatial extent of floodplain inundation, and measured flow velocities. Using the model results, we analyzed the flow in the river, spatial patterns of inundation, flow pathways, river-floodplain exchange, and water residence time on the floodplain. Our results highlight that bankfull flow is an oversimplified concept for explaining river-floodplain connectivity because some stream banks are overtopped and major low-lying floodplain channels are inundated roughly 19 days per year. As flow increased, inundation of floodplain channels at higher elevations dissected the floodplain, until the floodplain channels became fully inundated. Additionally, we found that river-floodplain exchange was driven by bank height or channel orientation depending on flow conditions. We propose a conceptual model of river-floodplain connectivity dynamics and developed metrics to analyze quantitatively complex river-floodplain systems.

1. Introduction

Most hydrologic and geomorphic models represent meandering river floodplains as relatively flat, featureless deposits adjacent to a river channel that may or may not include levees, point bars, and a sloping floodplain surface. This simple conceptualization appears in disciplines ranging from geomorphology (e.g., James, 1985; Lauer & Parker, 2008; Lauer & Willenbring, 2010; Nicholas et al., 2006; Pizzuto, 1987; Viparelli et al., 2013) to hydraulic engineering (e.g., review by Knight & Shiono, 1996; Sturm, 2001). Contrary to this simple conceptual model, high-resolution topographic data reveal that meandering river floodplains are remarkably complex and often contain channel networks that should enhance connectivity between rivers and their floodplains (David et al., 2017; Trigg et al., 2012). Still, the notion that floodplains are simple persists. In fact, the classical meandering river floodplain (type B3 in Nanson & Croke, 1992) is thought to form mostly by lateral channel migration, channel cutoff (creating oxbows), and overbank deposition (Fisk, 1944, 1947; Mackin, 1937; Wolman & Leopold, 1957), which has theoretically underpinned meandering river models for the past four decades (Bogoni et al., 2017; Camporeale et al., 2005; Eke et al., 2014; Hasegawa, 1977; Howard, 1992, 1996; Howard & Knutson, 1984; Ikeda et al., 1981; Johannesson & Parker, 1989; Motta et al., 2012a, 2012b; Odgaard, 1989a, 1989b; Schwenk et al., 2015; Seminara, 2006; Sun et al., 1996, 2001a, 2001b, 2001c). These simple models reinforce notions like bankfull flow (Leopold et al., 1964; Williams, 1978) that suggest connection of the main channel to the floodplain *only* occurs after a singular threshold in stage corresponding with bankfull discharge. Thus, the river corridor is reduced to a binary state of either flooded (discharge greater than bankfull) or channelized (discharge less than bankfull). Rather than a binary threshold process, we expect, based on existing topographic data and imagery (David et al., 2017; Mertes et al., 1996), that there exists a continuum of surface-water connectivity between rivers and their floodplains.

This continuum of connectivity can arise because meandering river floodplains often contain channels that convey water before all banks along the river channel are overtopped. These floodplain channels are not clearly accounted for in simple floodplain models (e.g., Nanson & Croke, 1992) and should directly influence river-floodplain connectivity. Floodplain channel networks are visible in satellite imagery (Lewin et al., 2017; Park & Latrubesse, 2017; Trigg et al., 2012), detailed laboratory experiments (van Dijk et al., 2012; van Dijk, van de Lageweg,et al., 2013; van Dijk, Teske, et al., 2013), and lidar data (David et al., 2017) and show complex channel network features on river floodplains (see review by Lewin & Ashworth, 2014). These channel networks are present in many river floodplains, such as along the Ogeechee River in Georgia (Benke et al., 2000), middle Amazon River in Brazil (Mertes et al., 1996; Trigg et al., 2012), Copper Creek in Australia (Fagan & Nanson, 2004), Kolymar River in Russia (Lewin & Ashworth, 2014), Congaree River in South Carolina (Kupfer et al., 2015), Sava River in Slovenia (Rak et al., 2016), and throughout many floodplains in Indiana (David et al., 2017). Detailed laboratory experiments show that the formation of scroll ridges and swales, channel cutoff, plugging of abandoned channels, and accretion on point bar complexes all contribute to complex floodplain topography (van Dijk et al., 2012; van Dijk, Teske, et al., 2013) and may play a role in enhancing or subduing floodplain channel networks and river-floodplain connectivity. High-resolution topographic data allow us to now look at floodplains in a way that was not possible in the past, revealing intricate erosion and deposition processes that lead to complex floodplain connectivity.

Floodplain channels affect hydrologic connectivity between the river and floodplain across a range of flows by transmitting water from the river across the floodplain and returning that water back to the river farther downstream. Connectivity, in this sense, relates to water-driven transport of matter, energy, and organisms between the river and floodplain (Amoros & Bornette, 2002; Bracken et al., 2013; Freeman et al., 2007). Hydrologic connectivity underpins river-floodplain exchange and affects water residence time, which are fundamental properties for understanding nutrient, organic material, and sediment retention by floodplains (Malard et al., 2002; Tockner et al., 1999) and along river corridors (e.g., Malard et al., 2000; Covino, 2017). These ideas on the importance of water moving from rivers into floodplains have been around for a while and have laid the foundations for river-floodplain connectivity (Amoros & Bornette, 2002; Junk et al., 1989; Ward & Stanford, 1995). Additionally, these floodplain channels are ephemeral, or intermittent, because they receive flow at a variety of times throughout the year. Intermittent channels can be hot spots of ecologic and hydrologic change and transformation (e.g., Datry et al., 2017). Presently, river-floodplain interactions that consider the continuum of connectivity or intermittency at a range of flows have not been rigorously quantified.

Our working hypothesis is that meandering rivers with floodplain channels will result in a range of flooding conditions because floodplain channels convey water and connect at a range of river discharges. This stands in contrast to the traditional notion of bankfull flow where flooding occurs only after a certain discharge (i.e., the binary or threshold-based floodplain definition). We focus exclusively on the surface-water component, and we discuss the implications this has for surface water connectivity and flow intermittency on floodplains. To test our hypothesis, we developed, calibrated, and validated a 2-D, surface-water hydrodynamic model using Hydrologic Engineering Center's River Analysis System (HEC-RAS) 2D to 32 km of floodplain (56 km along the river) of the East Fork White River near Seymour, Indiana, USA (drainage area of around 5,600 km^2). The 2-D hydrodynamic model results were used to assess the flow in the river channel, spatial patterns of inundation, flow pathways, river-floodplain exchange, and water residence time on the floodplain. Overall, we propose a conceptual model of river-floodplain connectivity dynamics and develop metrics to analyze quantitatively complex river-floodplain systems that could be applied in other systems.

2. Study Area

The White River Basin in Indiana drains roughly 29,400 km^2 of mostly agricultural lands (56% agriculture, 30% forested, and 11% urban; Homer et al., 2015). Historically, much of the White River Basin was forested, and during the 1800s, the land was cleared for agriculture (Crawford et al., 1996). The basin is split into two major drainages, the West Fork and the East Fork White River, that join near the outlet of the basin before draining into the Wabash River and then the Ohio River (Figure 1a). Both the Pre-Wisconsin and Wisconsin glacial limits fall within the basin, creating a north-south gradient in topographic relief.

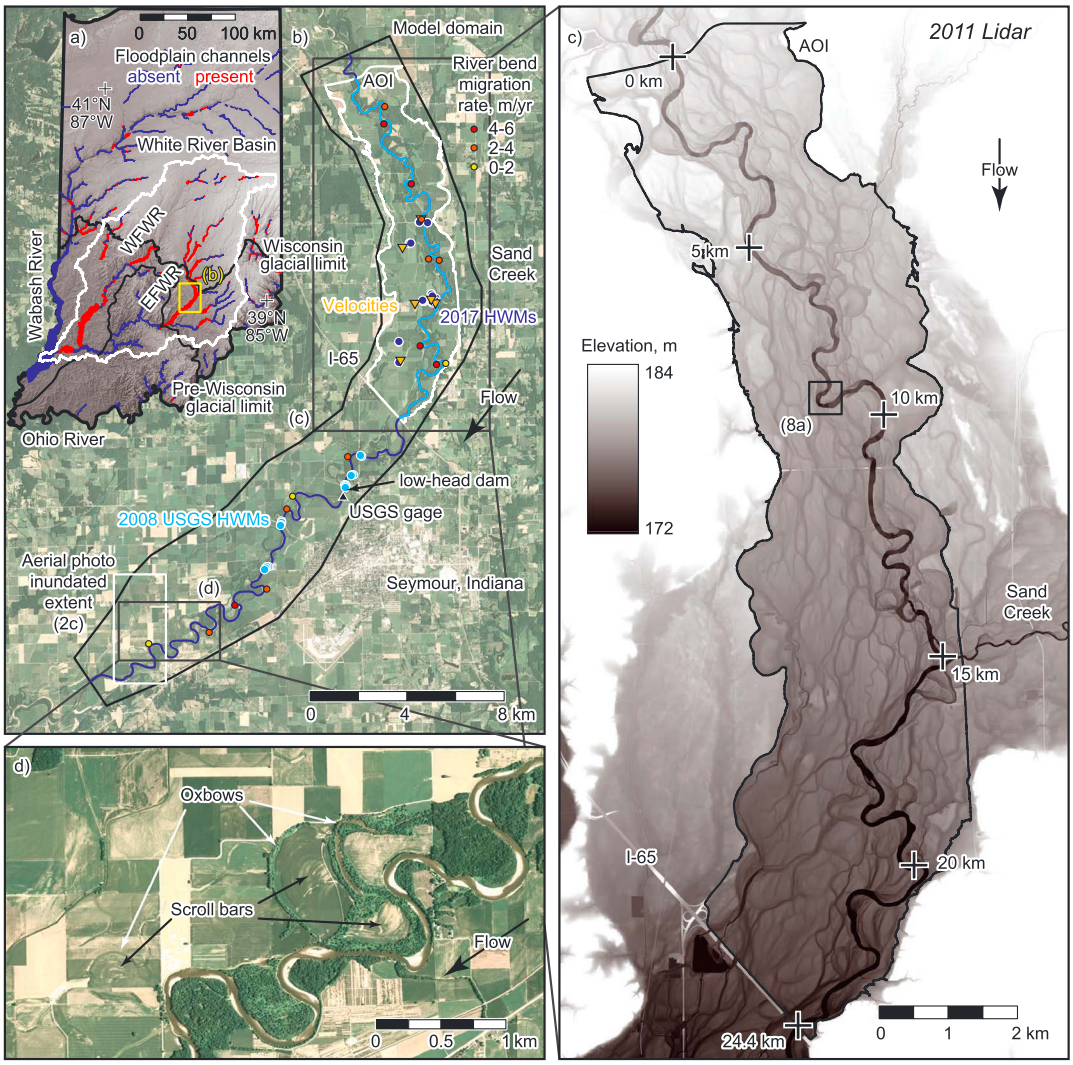

Figure 1. Study area of the East Fork White River and floodplain near Seymour, Indiana. (a) Location of the White River Basin in Indiana. Blue and red lines correspond to the identification of floodplains by David et al. (2017) where floodplain channels were absent and present, respectively. (b) Hydrodynamic model domain and area of interest (AOI) where results were reported. Model calibration data included elevation and discharge at the U.S. Geological Survey (USGS) gage (03365500). Model validation data included high-water marks (HWMs) collected in 2008 by the USGS and 2017 as part of this study, an aerial photo of inundated extent, and measured velocities in floodplain channels. Also shown are river bend migration rates from Robinson (2013). (c) Lidar data (from 23 March 2011) showing a network of floodplain channels within the AOI. (d) Reach highlighted by Brice (1974) showing the evolution of a compound meander loop.

The East Fork White River in Indiana is an archetype for a classical meandering river. Brice (1974) illustrated the evolution of a compound meander loop on a reach of this river (Figure 1d) with oxbows and scroll bars. Just upstream of this reach, the East Fork White River near Seymour, Indiana, meanders through an agricultural floodplain (Figures 1b and S1a in the supporting information). Lidar data reveal a complex and dense channel network on the floodplain of this meandering river (Figure 1c). While some of these floodplain channels appear to have formed from old oxbows, others appear to have formed from upstream migrating headcuts connecting floodplain lows (David et al., 2017, 2018). These floodplain channels are subtle features with low relief and are often indistinguishable from undulating topography in the field, but the flow conveyance through this network is large enough that a postflood imprint was left on the landscape along these channels whereas adjacent areas appeared unaffected (Figure S1c).

David et al. (2017) found floodplain channels in roughly 40% of floodplains throughout Indiana (in both glaciated and unglaciated terrain in areas with river-channel widths greater than 20 m, without heavy urbanization, and without straightened rivers; Figure 1a). In general, floodplain channels were found in fluvial

systems with large floodplain-to-river widths, high meandering rates, and predominantly agriculturally land use (David et al., 2017). The floodplain of the East Fork White River near Seymour, Indiana, is one of the more dramatic examples of a floodplain with channels (Figure 1c). The river channel here is roughly 90 m wide at the top of its banks, migrating at rates of up to 6 m/year (Robinson, 2013) through a roughly 2.7-km-wide floodplain (Figure 1b).

Our study area and model domain is roughly 32.2 km of floodplain along the river corridor, containing 55.7 km of the East Fork White River main channel, beginning downstream of Columbus, Indiana (drainage area of roughly 5,100 km^2), just below the confluence with Clifty Creek and extending nearly to Brownstown, Indiana (drainage area of roughly 6,100 km^2; Figure 1b). Within this reach, the only major tributary is Sand Creek (drainage area of roughly 670 km^2). There is a U.S. Geological Survey (USGS) streamflow-gaging station (03365500 East Fork White River at Seymour, Indiana) and low-head dam (see Figure 1b) near the middle of the model domain. This reach was chosen because of its extensive floodplain channel network, amount of data available for model calibration and validation, and numerous access points. Model results are only shown within an area of interest (AOI, roughly 14.3 km of floodplain, containing 24.4 km of river) in the upstream half of the model domain to avoid any uncertainties due to the low-head dam (Figures 1b and 1c). The AOI corresponds to the simulated extent of flooding at the peak of record on 8 June 2008 of 2,730 m^3/s. Within the AOI, land cover is 76% agriculture (predominantly corn and soybean), 13% forested, 7% open water, and 3% urban (Homer et al., 2015). Agricultural tile drainage is not prevalent in this floodplain presumably because the floodplain material is coarse enough to provide adequate drainage. The river slope is roughly 3.2×10^{-4} m/m computed along the main channel centerline, and floodplain slope is roughly 5.5×10^{-4} m/m computed from the average floodplain surface elevation along the floodplain valley centerline.

3. Methods

3.1. Topography and Bathymetry

The terrain surface was constructed from 1.5-m lidar data (OpenTopography, 2013) and surveyed river bathymetry. During postprocessing of the lidar data, areas where the lidar encountered water on the day of the survey (23 March 2011; gage water-surface elevation of 170.0 m; USGS, 2017) were hydro-flattened —a process by which a flat or sloping surface is enforced to represent a smoother water surface. The hydro-flattened surface was replaced by a bathymetric surface created from a boat survey of the river bed. River bathymetric data were collected on 11 and 18 October 2016 (gage water-surface elevations of 168.7 and 168.6 m, respectively; USGS, 2017) using a single-beam Lowrance Mark-4 depth sounder (for depth and spatial location). Data density captured the major pool-riffle sequences. During the survey, 60 water surface elevation (WSEL) data points were collected (roughly three at the same location every 1.5 river km) using a Leica Viva GNSS GS12 real-time kinematic global positioning system (RTK-GPS) (reported 3-D accuracy averaged for all points was 0.02 m) to convert depth to elevation. Bed elevations were computed by linearly interpolating (along the river channel centerline) the surveyed WSELs to each depth measurement and then subtracting the depth measurements from the interpolated WSELs. Next, all bed elevation data were averaged along the river channel centerline within 30-m increments (roughly half of the average river top width). The averaged bed elevations were then assigned along the entire hydro-flattened width and used to construct a triangulated irregular network for the extent of the hydro-flattened lidar surface area upstream of the low-head dam. Downstream of the low-head dam, the hydro-flattened lidar surface was lowered by 1.5 m, which was the same average offset as upstream of the dam (a comparison of simulated WSELs using river channel bathymetry that had been surveyed vs. obtained by an average lowering of a hydro-flattened lidar surface is shown in Figure S2). Finally, portions of roadways in the floodplain with culverts were removed from the lidar data because this version of 2-D HEC-RAS cannot incorporate hydraulic structures.

3.2. Model Construction

A 2-D unsteady hydrodynamic model of the East Fork White River and floodplain was constructed using 2-D HEC-RAS version 5.0.3 developed by the U.S. Army Corps of Engineers (Brunner, 2016). One of the main reasons 2-D HEC-RAS was chosen to model the East Fork White River and floodplain was because it incorporated a high-resolution subgrid model that generated geometric and hydraulic property tables for

cells and cell faces based on the underlying terrain (Brunner, 2016; Casulli, 2009). As a result, hydraulic computations incorporated the full resolution of the underlying terrain even when the computational grid was coarse, such that cells were partially wet and flood inundation mapping was at the resolution of the terrain.

Construction of the HEC-RAS model involved generating a computational mesh with a nominal orthogonal cell spacing of 15 m. Break lines were enforced along the river channel centerline and banks (with nominal cell spacing of 12 m), major floodplain channels and roadways (with nominal cell spacing of 3 m), and the crest of the low-head dam (with nominal cell spacing of 1.5 m). Overall, the computational mesh included over 585,000 cells with an average cell area of 210 m^2. The downstream boundary condition was set as normal depth, for which the computation required a friction slope, set at 0.001. Flow at the upstream boundary was specified as 90% of the flow at the USGS gage (03365500 East Fork White River at Seymour, Indiana); the remaining 10% entered from Sand Creek (roughly 15 river km downstream; as determined from flow records and comparing relative drainage areas; Figures 1b and 1c). Roughness values were assigned based on land cover (Homer et al., 2015) and with initially default Manning's n values for each land-cover class (Brunner, 2016). We simulated steady state conditions in 2-D HEC-RAS by holding a particular flow constant before incrementing to the next flow. Flows for calibration (as well as for model results) were chosen to span the stage-discharge rating curve from the 2008 peak flow (2,730 m^3/s) in 20 increments, representing 0.2-m changes in stage (Figure 2a and Table S1).

3.3. Model Calibration and Validation

The model was calibrated to the USGS rating curve (USGS, 2016) by only changing Manning's n values for the river channel (classified as open water) and agricultural lands. Our final calibrated Manning's n values for the river channel and agricultural lands were 0.033 and 0.05, respectively. The root mean square error (RMSE) of the calibrated model simulations of WSEL to the USGS rating curve was 0.12 m, with a mean absolute error (MAE) of 0.10 m ($n = 21$, where n is the number of values; Figures 2a, S3a, and S3b). For context, the USGS rating curve fit to the stage-discharge measurements had an RMSE of 0.25 m and MAE of 0.18 m ($n = 785$). Thus, the model error was within the uncertainty of the USGS streamflow measurements (Figures 2a, S3a, and S3b). Additionally, the largest errors were at low flow, but these errors were consistent with more recent (post-2000) USGS streamflow measurements (Figure S3b). Most importantly, the errors from our simulations were even lower (RMSE of 0.07 m and MAE of 0.06 m, $n = 14$) when the floodplain channels were flowing.

Model validation data included comparing results to surveyed high-water marks (HWMs), inundation in an aerial photo, and measured velocities in flowing floodplain channels (see locations in Figure 1b). HWMs were collected in 2008 by USGS around bridge abutments and corresponded to the peak flow of record on 8 June 2008 of 2,730 m^3/s (Morlock et al., 2008; USGS, 2017). We augmented this with HWMs collected on 3 March 2017 by surveying the debris (mostly corn stalks) stranded at local high points on the floodplain using the RTK-GPS (Table S2). The 2017 HWMs were associated with the highest flow during the winter on 21 January 2017 of 600 m^3/s (15-min peak; USGS, 2017). Model simulation results were more accurate for the 2017 HWMs (RMSE 0.24 m, MAE 0.19 m, $n = 27$) than for the 2008 USGS HWMs (RMSE 0.41 m, MAE 0.29 m, $n = 17$; Figures 2b, S3d, and S3e). The largest discrepancies between the model and the 2008 USGS HWMs occurred just upstream of the low-head dam and just upstream of the location where the river makes a sharp bend under a railroad bridge with several large piers. The hydraulics are complicated in this location, which was partially why we focused our results in an AOI farther upstream (Figure 1b).

An aerial photo showing the spatial extent of floodplain inundation was taken on 7 April 2011 around 12:30 pm EST and corresponds to an instantaneous (15 min) flow at the gage of 657 m^3/s and stage of 172.7 m (Figures 2c and S3f). This flow-stage clustered with the USGS streamflow measurements with WSELs less than predicted from the rating curve (Figure S3c). Therefore, model simulations were able to match either the flow (Table S3g) or the stage (Figures 2c and S3h). Our 2-D HEC-RAS model simulations were able to capture the extent of inundation of the floodplain channels in exceptional detail, and most accurately when matching the stage (Figures 2c and S3h). The uncertainty associated with calibration to the rating curve is visually translated to the spatial extent of inundation by comparing Figures S3g and S3h.

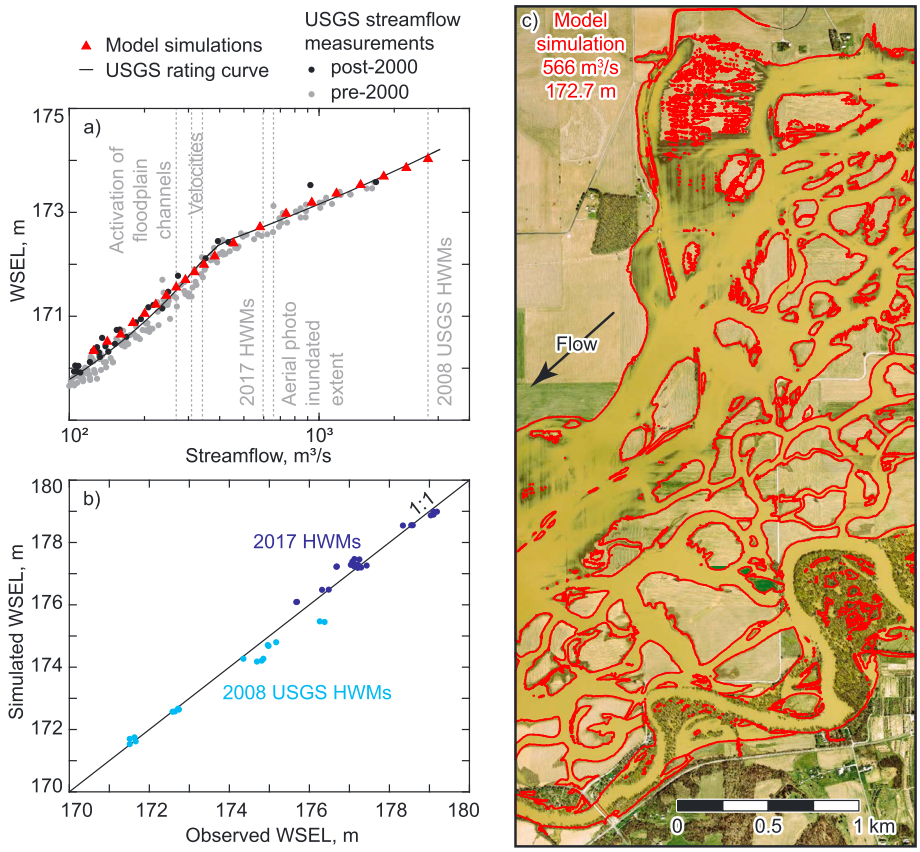

Figure 2. Calibration and validation of the two-dimensional hydrodynamic model. (a) Model calibration to the elevation-discharge rating curve at the U.S. Geological Survey (USGS) gage (location shown in Figure 1b). (b) Model validation against high-water marks (HWMs) collected in 2008 by the USGS and 2017 as part of this study (location of HWMs is shown in Figure 1b). (c) Aerial photo of inundation extent on 7 April 2011 (location is shown in Figure 1b). Model simulations of inundated extent, shown as red lines, correspond to the same water surface elevation (WSEL) as observed on 7 April 2011.

Velocities in flowing floodplain channels were measured on 1–2 May 2017 using a RiverRay Teledyne RD Instruments acoustic Doppler current profiler coupled with a Hemisphere A325 differential global positioning system (GPS) from a tethered boat following standard USGS procedures for routine discharge measurements (Mueller & Wagner, 2009). At six sites (Figure 1b), velocity data were collected from a combination of cross sections, stationary profiles, and longitudinal profiles within floodplain channels. Concurrently, WSELs in the floodplain channels were measured using the RTK-GPS. Velocity data were processed using the Velocity Mapping Toolbox (Parsons et al., 2013) to export a depth-averaged velocity at the location of each velocity profile measurement.

Prior to data collection, on 30 April 2017, the flow at the gage peaked at 481 m^3/s (15-min value). During data collection, the flow in the river receded to 334 m^3/s by 1 May and 307 m^3/s by 2 May 2017 (both daily mean values). There were large uncertainties in comparing these measurements to model simulations because the measurements captured a snapshot of the transient receding flood wave and not a steady state condition for which this model was developed. Both groundwater interactions (Mertes, 1997) and time delays between the stage in floodplain channels and in the river at the downstream gage contributed largely to these uncertainties. As such, we felt that the most appropriate way to compare these measurements to our model was to first determine which flow simulation best matched WSELs in the floodplain channels and then, for that flow, compare velocities. This corresponded to a flow of 454 m^3/s at the gage; at this flow the difference between the simulated and measured WSELs had an RMSE of 0.16 m, MAE of 0.13 m, and standard deviation of 0.13 m (n = 72). Furthermore, at this flow, the difference between the simulated (average = 0.31 m/s at measured points) and

measured (average = 0.45 m/s) velocities had an RMSE of 0.27 m/s, MAE of 0.21 m/s, and standard deviation of 0.24 m/s (n = 15,705). Besides, the uncertainty in comparing steady state model simulation results to flood-recession measurements, probably the largest errors in the velocity comparison arose from the discrepancy between the spatial and temporal scales of the velocities. Velocity measurements had a spatial scale from the acoustic Doppler current profiler beam footprint (comparable to the flow depth, ~1 m) and timescale of less than a second such that these were instantaneous turbulent values, whereas velocity simulations had a spatial scale of the model grid cell (which varied depending on whether the grid was refined in all of the floodplain channels but would be at least 3 m) and represent time averages. Therefore, we cannot expect good agreement between the simulation and measurements of velocities. Interestingly, the WSELs and velocities in the floodplain channels were most accurately simulated with a flow closer to the peak flow a day or two earlier rather than the flow on the date of the survey. This may suggest that the flood wave propagates much slower through the floodplain channels than it does in the river, although given the model uncertainty, this warrants further field investigation.

3.4. Model Simulations and Analytical Methods

Model simulations were performed for 21 steady state flow conditions with recurrence intervals provided in Table S1. The daily flow exceedance probability at the USGS gage (03365500 East Fork White River at Seymour, Indiana) for water years 1928–2016 was calculated with daily flow data using a Weibull plotting position formula (Interagency Committee on Water Data (IACWD), 1982) and is shown in Figure 3. Daily flow data allowed us to compute daily and monthly recurrence intervals for frequent flows as well as the number of days the flow was exceeded per year (Table S1). It is important to note that there is a strong seasonality to the recurrence of floodplain inundating flows, with many of the floodplain channels most likely wetted during most of March and April (Figure 3).

Primary model results were depth/WSEL and 2-D velocity, upon which all subsequent analyses were based. Model results were interpolated to a 15-m grid (coincident with the nominal orthogonal grid locations of cell faces) for consistency because depth/WSEL data were reported at cell centers and 2-D velocity data were reported at cell faces. At each grid location m and for each flow ξ, we calculate the 2-D specific discharge $\boldsymbol{q}_m^{\xi}$ [$L^2\ T^{-1}$] (or discharge per unit width; a 2-D vector indicated by bold font) as

$$\boldsymbol{q}_m^{\xi} = \boldsymbol{v}_m^{\xi} * h_m^{\xi}, \tag{1}$$

where $\boldsymbol{v}_m^{\xi}$ [LT^{-1}] is the depth-averaged 2-D velocity and h_m^{ξ} is the water depth.

Flow in the river channel was determined by integrating the component of $\boldsymbol{q}_m^{\xi}$ normal to a cross-section line. Cross sections were spaced every 33.5 m (roughly a third of the width of the river channel at the top of its banks) along the river-channel centerline (downstream distance was referenced to the upstream boundary). This created a spatial series of $\boldsymbol{q}_m^{\xi}$ that was compared to the total flow input to the model domain. The variability of this series was summarized by the coefficient of variation as the standard deviation divided by the mean. The position of the left and right bank lines was determined by manually digitizing the highest elevations adjacent to the river channel. These bank lines mark the river channel-floodplain boundary. The WSEL along the river-channel centerline was compared to the elevation of both banks to determine if the banks were overtopped. The percentage of the banks overtopped for each simulated discharge is expressed relative to the total length of both banks.

Islands were defined as dry areas fully enclosed by floodwater. For each simulated flow, there was a distribution of island sizes, for which we reported the maximum, 90th percentile, 75th percentile, and median island size (area), as well as the total number of islands. We report the percentage of the floodplain area covered by islands, water, and by both islands and water relative to the extent of the AOI (as determined from the lateral extent of inundation at the highest simulated flow). Streamlines were generated from the 2-D velocity field, for visualization purposes, by tracing the trajectories of 100 particles distributed evenly along a cross section near the upstream end of the AOI.

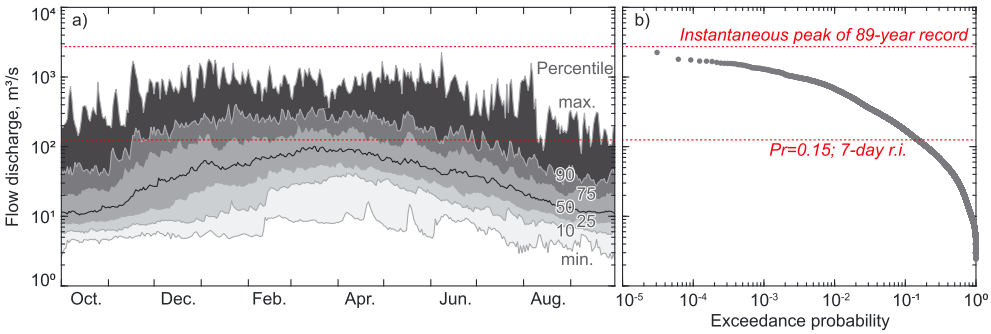

Figure 3. Daily flow exceedance probability at the U.S. Geological Survey gage (03365500 East Fork White River at Seymour, Indiana) for water years 1928–2016. (a) Flow exceedance for each day of the water year. (b) Flow exceedance for the entire period of record. Horizontal red dashed lines bracket the range of flows simulated in the model (see Table S1 for specific flows) with reported probability of exceedance (Pr) and recurrence interval (r.i.). This range of flows was chosen to focus on floodplain inundation.

A flow-integrated network of flow paths was constructed for the floodplain. We did this by first finding the centerlines of inundated channel features at the lowest flow (these features became the first links of the network). A channel feature was defined as a connected wet area separated from other connected wet areas by a dry island. At the next higher flow, newly inundated channel features were traced, and this procedure continued for all simulated flows and ended with the construction of a flow-integrated network of flow paths. Finally, the network was broken into individual links between junctions each with index i. Relevant attributes for each link of this network included link length ℓ_i [L], the flow index at which the link becomes activated ξ_i, and the velocity in link i at flow index ξ as v_i^{ξ} [LT^{-1}], which was computed by averaging the velocity magnitude along the length of the link at a particular flow. For this network, we reported the total length of newly activated flow paths ℓ_ξ [L] at a given flow ξ as

$$\ell_\xi = \sum_{i:\xi_i=\xi} \ell_i \tag{2}$$

and the total cumulative length of all flow paths L_ξ [L] that were activated at or below a given flow ξ as

$$L_\xi = \sum_{i:\xi_i\le\xi} \ell_i. \tag{3}$$

Downstream distance was calculated along the river channel centerline unless otherwise noted. Where cross sections and bank lines intersect, nine additional uniformly spaced points were created between adjacent points to increase the resolution to quantify river-floodplain exchange. The lateral flux per unit width (or lateral unit flux) across the bank $q_j^{\xi,B}$ [$L^2\,T^{-1}$] was calculated at the location of all points (with index j) along the bank (with index B, either L for left bank or R for right bank) as the component of the 2-D specific discharge $\boldsymbol{q}_m^{\xi}$ that is transverse (or parallel) to the channel cross section. For the additional points, which were not associated with a specific cross section, the transverse direction was interpolated from the upstream and downstream cross sections to decompose the vector. An average streamwise flux per unit width (or streamwise unit flux) in the river channel q_c^{ξ} [$L^2\,T^{-1}$] (where the subscript c denotes the river channel) was calculated as the average magnitude of the 2-D specific discharge $\boldsymbol{q}_m^{\xi}$ over all grid locations m within the river channel as

$$q_c^{\xi} = \overline{\left\|\mathbf{q}_m^{\xi}\right\|}_{m\in river}. \tag{4}$$

We computed a normalized, smoothed lateral unit flux $\tilde{q}_j^{\xi,B}$ for each bank by smoothing the lateral unit flux series $q_j^{\xi,B}$ with a 67-m moving window (twice the distance between cross sections; smoothed over 21 bank points) and normalizing by the average streamwise unit flux q_c^{ξ} to contextualize the resulting values as

$$\widetilde{q}_j^{\xi,B} = \left(\frac{1}{21}\sum_{j-10:j+10} q_j^{\xi,B}\right)\frac{1}{q_c^{\xi}}. \quad (5)$$

Positive values of $q_j^{\xi,B}$ or $\widetilde{q}_j^{\xi,B}$ denote lateral unit fluxes into the channel and negative values denote lateral unit fluxes into the floodplain.

The normalized, smoothed lateral unit flux series $\widetilde{q}_j^{\xi,B}$ was correlated with a relative bank height and channel orientation. Relative bank height was computed for both banks by detrending a series of simulated WSELs along the river centerline at a moderate flow (454 m^3/s) from a series of elevations along the top of each bank. The result is a series of highs and lows in bank elevation relative to a simulated WSEL. Channel orientation was computed as the angle (clockwise direction is positive) from the direction of the channel centerline to the direction of the floodplain centerline. Additionally, the series of relative bank height was cross-correlated with channel orientation to assess how strongly these two factors covary and to provide context for the significance of the correlations between these series and the flux series.

An average lateral exchange across each bank $q_{ex}^{\xi,B}$ [$L^2\,T^{-1}$] was computed by integrating (via the trapezoidal approximation) the absolute values of the lateral fluxes across each bank line (using actual distances, not stationing) and then dividing by the total length along the bank as

$$q_{ex}^{\xi,B} = \left(\frac{1}{2}\sum_j \left|q_j^{\xi,B} + q_{j+1}^{\xi,B}\right| d_{j:j+1}^{B}\right)\frac{1}{D^B}, \quad (6)$$

where $d_{j:j+1}^{B}$ [L] is the along-bank distance between points j and $j+1$ and D^B [L] is the total length along bank B computed as

$$D^B = \sum_j d_{j:j+1}^{B}. \quad (7)$$

We took the absolute value here because we wanted to account for all crossings across the river-floodplain boundary instead of a net value (without the absolute value), which is expected to be close to zero. While this may seem like double counting, each boundary crossing likely includes water that has been mixed in the river or floodplain channels with other water before the next boundary crossing. By exchange, we only refer to lateral surface-water, river-floodplain exchange.

To summarize and normalize exchange, river-floodplain exchange $\widetilde{q_{ex}^{\xi}}$ was calculated by adding the average lateral exchange across both banks $q_{ex}^{\xi,L}$ and $q_{ex}^{\xi,R}$ and dividing by the average streamwise unit flux q_c^{ξ} as

$$\widetilde{q_{ex}^{\xi}} = \frac{q_{ex}^{\xi,L} + q_{ex}^{\xi,R}}{q_c^{\xi}}. \quad (8)$$

An average velocity in the river channel v_c^{ξ} [LT^{-1}] was calculated as the average magnitude of the 2-D velocity $\boldsymbol{v}_m^{\xi}$ over all grid locations m within the river channel as

$$v_c^{\xi} = \overline{\left\|\mathbf{v}_m^{\xi}\right\|_{m\in river}}. \quad (9)$$

An average velocity in the floodplain v_f^{ξ} [LT^{-1}] (where the subscript f denotes the floodplain) was calculated as the length-averaged velocity of links in the cumulatively activated flow path network as

$$v_f^{\xi} = \frac{1}{L_\xi}\left(\sum_{i:\xi_i\le\xi} v_i^{\xi}\ell_i\right). \quad (10)$$

A residence time per unit length in the river t_c^{ξ}[T] and floodplain t_f^{ξ} [T] was calculated as the inverse of their respective velocities as

$$t_c^{\xi} = \frac{1}{v_c^{\xi}} \tag{11}$$

and

$$t_f^{\xi} = \frac{1}{v_f^{\xi}}. \tag{12}$$

By residence time, we only refer to surface-water residence times in the river or floodplain. To normalize residence time, floodplain residence time $\widetilde{t_f^{\xi}}$ was computed by dividing the residence time per unit length in the floodplain t_f^{ξ} by that of the river t_c^{ξ} as

$$\widetilde{t_f^{\xi}} = \frac{t_f^{\xi}}{t_c^{\xi}}. \tag{13}$$

4. Results

Inundation of the lowest elevation floodplain channels along the East Fork White River occurred roughly 19 days per year (268 m^3/s, 19-day recurrence interval (r.i.); Figure 4a). Often, a single storm event raises water elevations in floodplain channels high enough to inundate these channels for multiple days, with the highest probability of occurrence during winter or spring (Figure 3). When active, these floodplain channels convey water through several corridors spanning the floodplain-valley walls (initially at 268 m^3/s; Figure 4a). As flow increases, the floodplain becomes more dissected (i.e., where water in channels cut across the floodplain) and more highly connected as water inundates floodplain channels at higher elevations (Figure 4a). At even higher discharges, the inundated areas coalesce and fully cover the floodplain (above 935 m^3/s, 9-month r.i., exceeded 1.4 days per year; Figure 4a). Generally, as flow increases, velocity also increases (Figure 4b). The exception, though, is where the river channel is oriented transverse to the direction of floodplain flow. In these locations, velocities in the river channel decrease at the highest flows, and in some instances, so much that the velocities on the adjacent floodplain were higher than in the river channel (see star, Figure 4b).

The simulated discharge in the river channel fluctuated downstream as water was exchanged between the river and floodplain (Figure 5). At low flows, such as 268 m^3/s (Figures 5b–5d), the flow in the river channel conveyed nearly all the input specified at the upstream boundary. With the exception of flow into two cutoffs (Figure 5b), any discrepancies between the flow in the river channel and the input flow were small and resulted from uncertainty in aligning cross sections normal to the flow direction. At higher flows, there was more river-floodplain exchange and the amount of flow conveyed in the river channel fluctuated significantly (Figures 5a, 5c, 5d, and 5e). For instance, at 935 m^3/s, the river channel conveyed only half of the total flow with the other half being conveyed in floodplain channels. Whereas at 2,730 m^3/s, only roughly 25% of the total flow was conveyed in the river channel (Figure 5d). The flow variability in the main channel was caused by river-floodplain exchange, and this was partly driven by the variability of bank height, which had a standard deviation of 0.7 m (Figures 5c and 6a). This large variability in bank height resulted in frequent overtopping that occurred gradually over a large flow range, which made it difficult to define bankfull flow (Figure 6b).

Inundation of the floodplain along the East Fork White River created floodplain islands (Figures 7e and S4). The largest islands were created after the first major floodplain channels became inundated (268 m^3/s); island size decreased as flow increased and filled more channels (Figures 7a, 7e, and S4). Interestingly, for flows between 268 and 454 m^3/s there was a larger proportion of dry floodplain (islands) than areas inundated by water (Figure 7f). A flow of 581 m^3/s (2.4-month r.i., exceeded 5 days per year) represented the maximum dissection of the floodplain, as this flow created the most islands (Figure 7b). At this flow, there was also a peak in the total length of activated flow paths (Figure 7c). The number of islands plateaued because as stage increased, floodwaters inundated higher elevations near the valley margins (creating new islands) and fully inundated low-lying areas (removing islands; Figure 7f). At 935 m^3/s (9-month r.i., exceeded 1.4 days

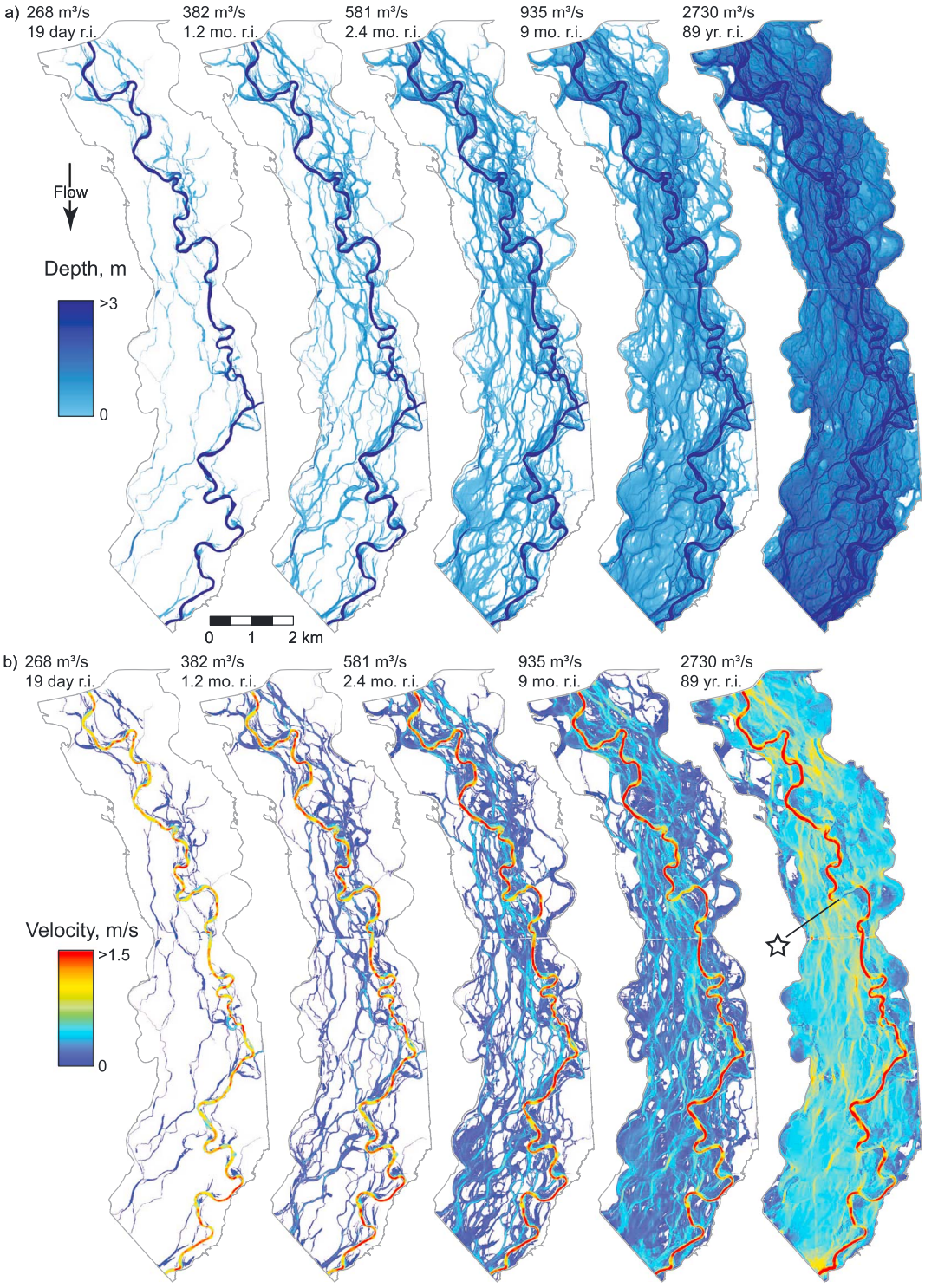

Figure 4. Model simulation results of (a) depth and (b) velocity within the area of interest. The star in (b) for flow 2,730 m^3/s indicates higher velocities on the adjacent floodplain than in the river channel. Simulated flows are listed with recurrence interval (r.i.).

per year), the floodplain was fully inundated (Figures 7e and S4), and floodplain dissection had decreased significantly (Figure 7).

Even after the floodplain was fully inundated, the locations of floodplain channels dictated flow pathways on the floodplain (Figure S5). At 2,730 m^3/s, the flow pathways were much straighter and generally

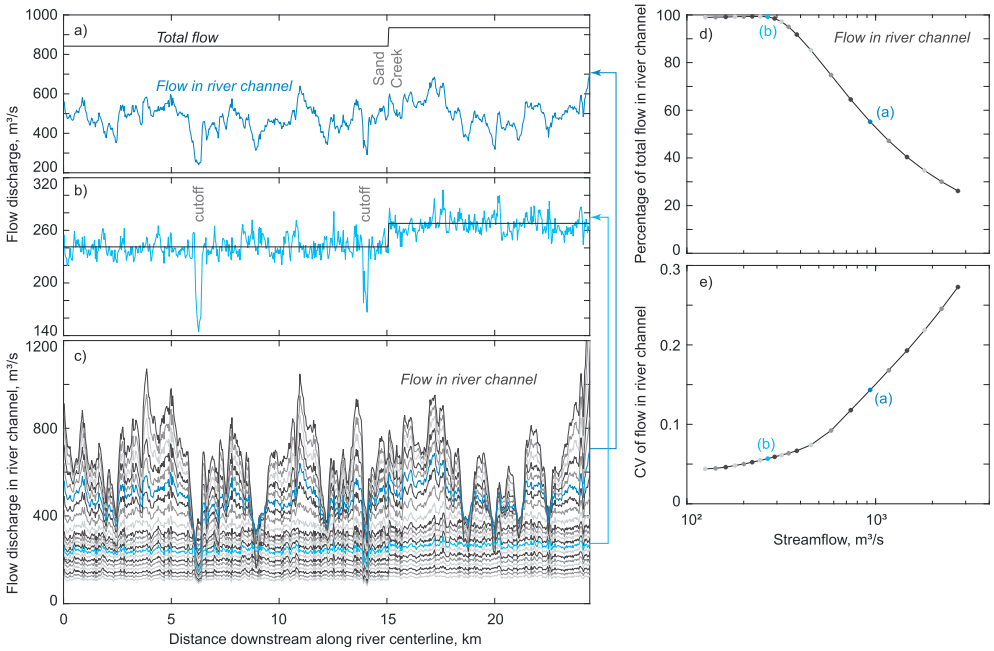

Figure 5. Simulated discharge within the river channel of the East Fork White River in the area of interest at (a) 935 m^3/s, 9-month recurrence interval, (b) 268 m^3/s, 19-day recurrence interval, and (c) for all 21 simulated flows. Solid black lines in (a, b) denote the total flow input into the model domain. (d) Percentage of total flow in the river channel. (e) Coefficient of variation (standard deviation divided by the mean) of the river-channel, flow-discharge series along the river centerline.

oriented down valley, suggesting that the floodplain topography had minimal influence on flow pathways. Interestingly, at higher flows the flow pathways occupied a narrower corridor along the floodplain because at larger depths the role of channels shifted from routing and dispersing flow across the floodplain to becoming roughness elements (flows above 1,816 m^3/s, 45-year r.i.; Figure S5).

The lateral unit flux across the river-floodplain boundary increased with increasing flow (Figures 8 and S6). Often, a flux into the channel across one bank was accompanied by a flux into the floodplain across the other bank. This can be seen across an individual meander bend (Figures 8a, S6b, S6d, and S6f) and also for the entire reach where positive values of flux across one bank coincided with negative values of flux across the other bank (recall positive values denote fluxes into the channel and negative values denote fluxes into the floodplain; Figures 8b, S6c, S6e, and S6g). The structure or variability of the downstream series of lateral unit flux is related to relative bank height (which includes lows in the banks where floodplain channels connect to the river channel; Figure 6a) and channel orientation (Figure 8d). For lower flows that barely

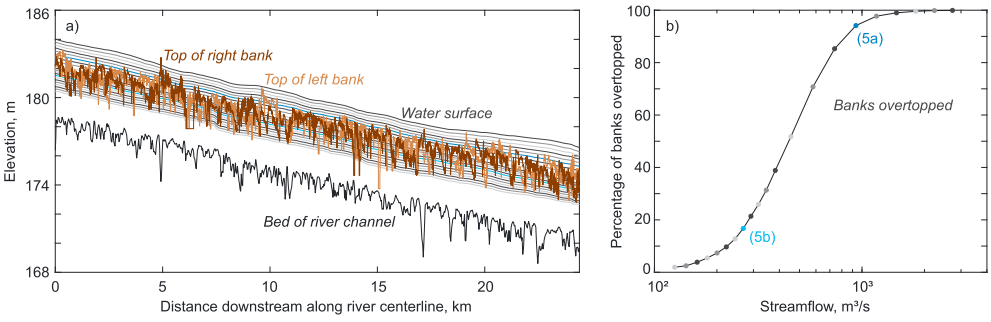

Figure 6. Assessment of bankfull flow. (a) Bed, bank, and water surface elevation profiles for all 21 simulated flows. (b) Percentage of banks (by total length for both banks) overtopped by each simulated discharge.

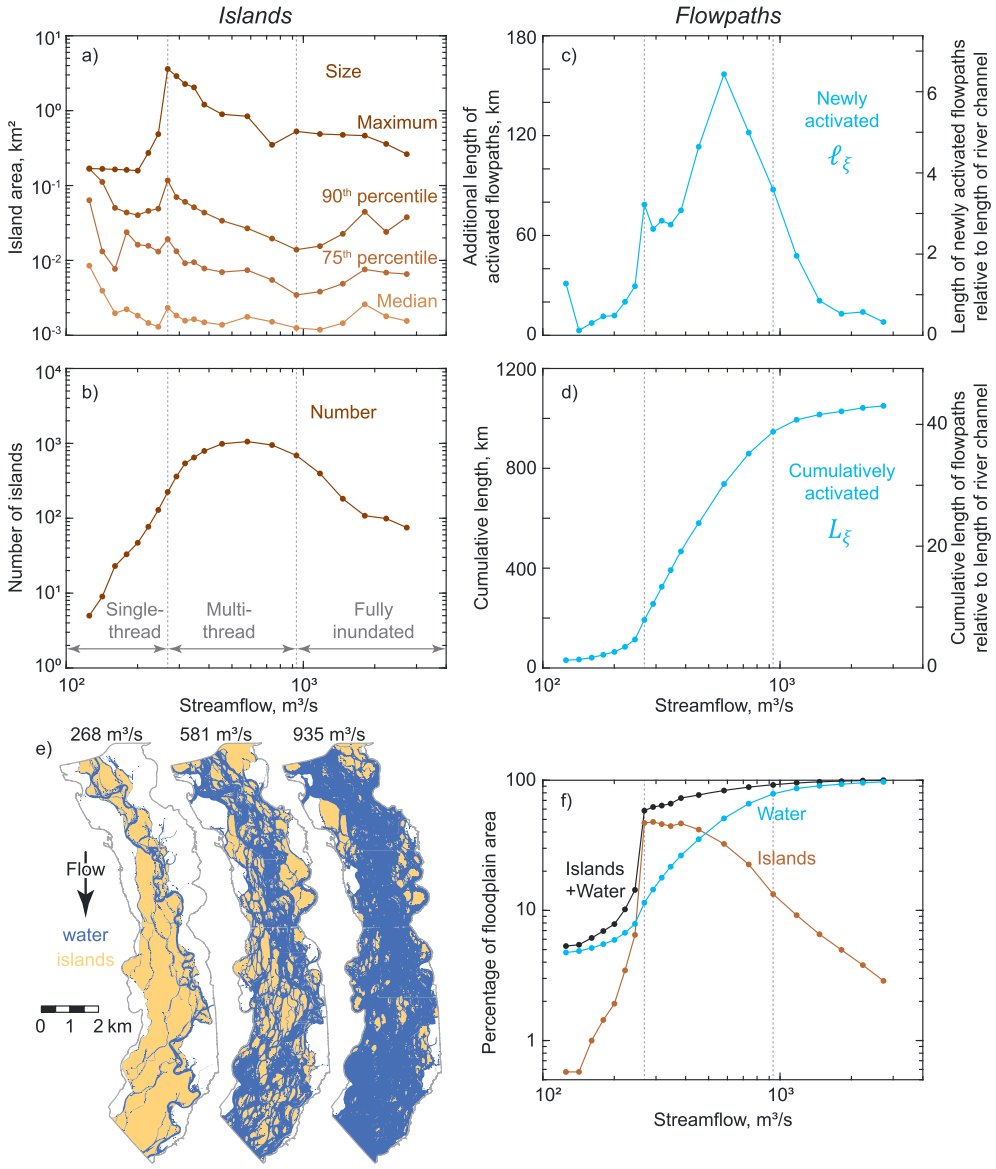

Figure 7. Island and flow-channel network statistics over a range of flows. (a) Statistics of island size (area). (b) Number of islands formed. (c) Additional length of newly activated flow paths ℓ_ξ at flow ξ. (d) Total cumulative length of all flow paths L_ξ. (e) Dissection of the floodplain by floodwaters into islands at moderate flows. (f) Percentage of the total floodplain area within the area of interest that was covered by islands, water, or islands and water. Vertical dashed gray lines separate three qualitatively different river-floodplain regimes: single thread, multithread, and fully inundated.

inundate the floodplain, relative bank height explains more of the structure of the downstream series of lateral unit flux than channel orientation (Figure 8c), with a peak correlation at 382 m^3/s (1.2-month r.i., exceeded 10 days per year). This occurs because initially water enters the floodplain at local lows in the bank. At high flows, channel orientation becomes more important (Figure 8c), driving flow across the river-floodplain interface wherever the channel direction is oriented transverse to the direction of floodplain flow (Figures 8d and S6a). The crossing point between these two regimes is at 581 m^3/s (2.4-month r.i., exceeded 5 days per year).

Any floodplain can have its surface-water hydraulics distilled down to a quantification of exchange (Figure 9a) and water residence time (herein as simply a unit length scale divided by velocity; Figure 9b). To generalize our results, we normalized floodplain exchange and residence time relative to values for the river channel (see equations (7) and (12); Figure 9c). For the East Fork White River, at 454 m^3/s (1.6-

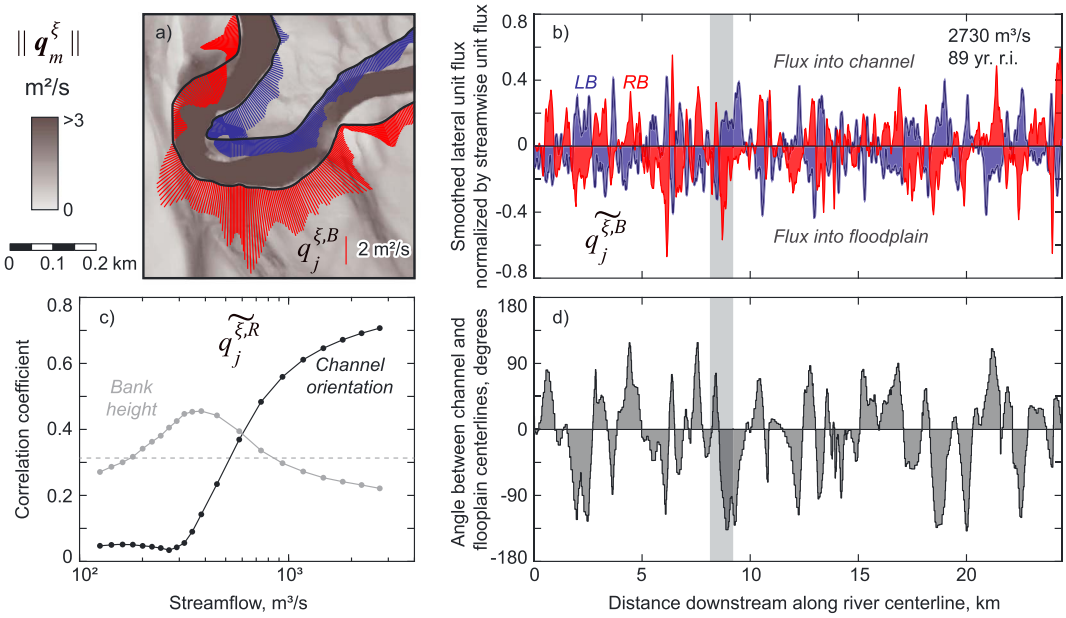

Figure 8. River-floodplain exchange. (a) Exchange of water between the river channel and the floodplain at (a, b) 2,730 m^3/s, peak of 89-year record. (a) Inset area showing the magnitude of the 2-D specific discharge $\|\boldsymbol{q}_m^{\xi}\|$ (gray contour) across the floodplain, top of bank (black lines), vectors of lateral unit flux $q_j^{\xi,B}$ across the right bank (RB; red) and left bank (LB; dark blue); see Figure 1c for location. (b) Normalized, smoothed lateral unit flux $\widetilde{q_j^{\xi,B}}$ across both banks. Positive values denote fluxes into the channel, and negative values denote fluxes into the floodplain. Gray highlighted section corresponds to the area shown in (a). (c) Correlation of the series of normalized, smoothed lateral unit flux across the right bank $\widetilde{q_j^{\xi,R}}$ (red lines in b) with the series of relative right bank height (Figure 6a) and channel orientation (d). Gray dashed line signifies the correlation between relative right bank height and channel orientation. (d) Angle from the direction of the channel centerline to the direction of the floodplain centerline (clockwise direction is positive).

month r.i., exceeded 7.7 days per year), roughly 10% of the streamwise flux in the river exchanged laterally across the river-floodplain interface, increasing to 30% at 2,730 m^3/s (peak of 89-year record; Figure 9c). Once water entered the floodplain at 268 m^3/s (19-day r.i., exceeded 19 days per year), it stayed there 30 times longer than it would have if conveyed within the river channel compared to three times longer at 2,730 m^3/s (peak of 89-year record; Figure 9c).

5. Discussion

5.1. Bankfull Flow Is an Oversimplified Concept for Explaining River-Floodplain Connectivity

The concept of bankfull flow assumes that floodplains become inundated when flow stage exceeds the banks, and this flow stage usually recurs every 1 to 2 years (Leopold et al., 1964; Williams, 1978). For the East Fork White River near Seymour, Indiana, the concept of bankfull flow seemingly does not apply because of the variability in bank height and the wide range of flows (268–935 m^3/s, 19-day to 9-month r.i., exceeded 19–1.4 days per year) where banks were overtopped (Figure 6). Similar findings were also reported for the Ogeechee River in Georgia (Benke et al., 2000) and the Congaree River in South Carolina (Kupfer et al., 2015). Instead of the binary concept of bankfull flow, our results suggest there is a gradient of flooding activity across a range of flows. For rivers with a defined bankfull flow, we would expect to see a step function in the relation between flow and percentage of banks overtopped (Figure 6b). Instead, we observed a smooth transition zone where progressively more banks became overtopped.

The lowest-lying floodplain channels were inundated roughly 19 days per year (Figure 4a, 268 m^3/s, 19-day r.i.), forming large islands (Figures 7a, 7e and S4). This flow also marked the beginning of increased bank overtopping (Figure 6b) and floodplain flow conveyance (Figure 5d). For roughly 5 days per year (581 m^3/s, 2.4-month r.i.), flooding in floodplain channels maximized dissection of the floodplain (Figures 7b and 7c), and this marked a regime shift between bank-height-driven and channel-orientation-

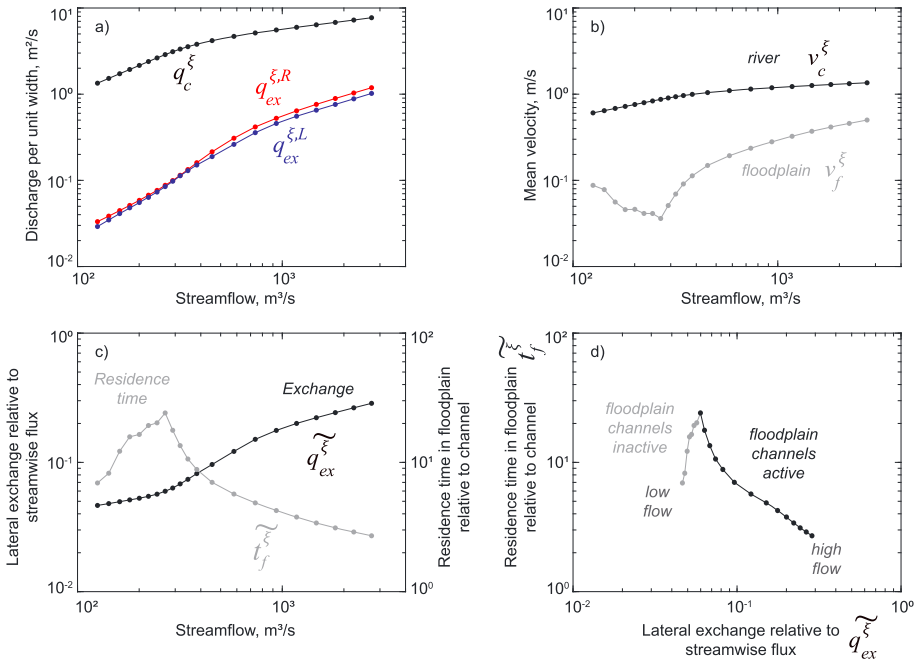

Figure 9. River-floodplain exchange and residence time. (a) Average streamwise unit flux in the river channel q_c^{ξ} (black) and average lateral exchange across the right bank $q_{ex}^{\xi,R}$ (red) and left bank $q_{ex}^{\xi,L}$ (dark blue). (b) Average velocity in the river channel v_c^{ξ} (black) and floodplain v_f^{ξ} (gray). (c) Lateral river-floodplain exchange normalized by the streamwise flux $\widetilde{q_{ex}^{\xi}}$ (black) and residence time in the floodplain normalized by the residence time in the river channel $\widetilde{t_f^{\xi}}$ (gray). (d) Mapping of the values in (c) into exchange-residence time space for the East Fork White River and floodplain. Values are colored by active floodplain channels (black) and inactive floodplain channels (gray).

driven river-floodplain exchange (Figure 8c). For roughly 1.4 days per year (935 m^3/s, 9-month r.i.), the floodplain was mostly inundated (Figure 4a), the banks were overtopped (Figure 6b), the floodplain conveyed roughly 50% of the total flow (Figure 5d), and increased flow beyond this point resulted in fewer islands (Figure 7b). This dissection of the floodplain into islands that were eventually inundated at high flows was similar to the dissection of braid bars investigated on the Platte River, Nebraska, by Limaye (2017). The floodplain is more or less completely inundated at recurrence intervals of 9 months and 1.7 years (Figure 4a). At these flows, most river-channel banks (Figure 6b) and floodplain-channel banks (Figure 4a) were overtopped. Interestingly, this corresponds to the recurrence interval around which traditional bankfull flow occurs (between a 1- and 2-year r.i.; note that for the West Fork White River at Newberry, Indiana bankfull flow was reported at a 1.1-year r.i., Leopold et al., 1964).

5.2. A Conceptual Model of River-Floodplain Connectivity Dynamics in Low-Gradient, Meandering Rivers

The concept of bankfull flow assumes that low-gradient, meandering river-floodplain systems transition directly from single thread to fully inundated at a certain discharge. Based on the results here and previous work (e.g., Benke et al., 2000; Kupfer et al., 2015), we emphasize that surface-water connectivity (via multithread floodplain channels) between the river and its floodplain is activated across a range of flows. This gradient of activation means that as highly connected meandering rivers flood, they transition between three distinct flow-dependent regimes: single thread, multithread, and fully inundated (Figure 10a). For the single-thread regime, the flow is conveyed within the main river channel. For the multithread regime, the flow is conveyed through a number of floodplain channels in addition to the main river channel (this regime occurs roughly 5% of the time for the study reach). For the fully inundated regime, water covers most of the floodplain (this regime occurs roughly 0.4% of the time). However, this general classification is not perfect, as the boundaries from one regime to the other are fuzzy. For instance, when transitioning from the single-thread to multithread regime, initially low areas in the floodplain become inundated, but they may not be

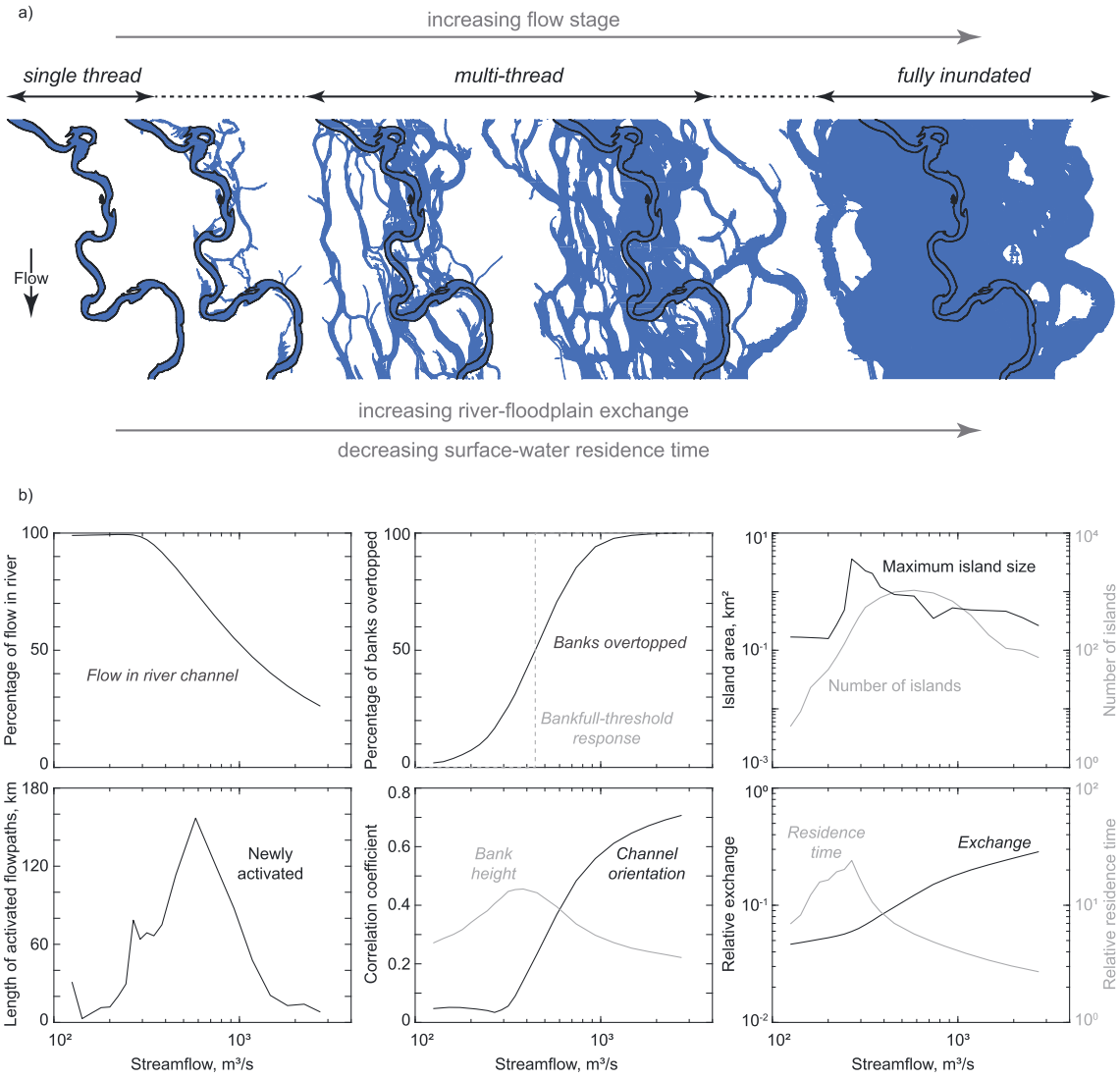

Figure 10. Conceptual model and framework for quantitatively analyzing river-floodplain connectivity dynamics. (a) Conceptual model of lateral surface-water, river-floodplain connectivity where low-gradient, meandering river-floodplain systems are classified as having three, flow-dependent regimes: single thread, multithread, and fully inundated. (b) Quantitative metrics for analyzing the connectivity of complex river-floodplain systems.

well connected to effectively convey flow. Transitioning from the multithread to the fully inundated regime, there may not always be complete inundation of the floodplain as ever higher floodplain channels become inundated, creating new floodplain islands. The generality of this style of floodplain is unknown, but given their widespread occurrence (Benke et al., 2000; David et al., 2017; Fagan & Nanson, 2004; Kupfer et al., 2015; Lewin & Ashworth, 2014; Mertes et al., 1996; Rak et al., 2016; Trigg et al., 2012), we suspect that as lidar data of floodplains becomes more common, more floodplains will be identified as having floodplain channels.

We envision that a useful paradigm for river-floodplain connectivity dynamics is within a quantifiable exchange-residence time framework that can serve as a process-based way to compare the functioning and connectivity of different floodplains (Figure 9d). Exchange flux and residence time are fundamental properties describing the strength of connectivity between the river and floodplain. The shape of this characteristic curve in exchange-residence time space should vary for different floodplains and resemble the structural and process-based controls governing river-floodplain connectivity and the underlying river-floodplain hydraulics. However, it remains to be seen how different floodplains plot in this exchange-

residence time space. We can illustrate how this framework can be used in the future for thinking about floodplain restoration. For instance, a goal of floodplain restoration might be to enhance exchange and residence time (Bryant-Mason et al., 2013; Forshay & Stanley, 2005; Tockner et al., 1999), thus selecting a floodplain design that plots farthest to the upper right in a graph of exchange versus residence time would be desirable (given several different curves representing different floodplain configurations in Figure 9d). However, there is a trade-off between exchange and residence time because as one increases, typically the other decreases (e.g., Findlay, 1995, and Figure 9d).

Overall, we have developed metrics for quantitatively analyzing complex river-floodplain systems. This includes analyzing the flow in the river channel, bank overtopping, floodplain-island statistics, length of flow paths, correlation between river-floodplain exchange and both bank height and channel orientation, floodplain residence time, and river-floodplain exchange (Figure 10b). Together, these metrics provide a quantitative overview of a river-floodplain system and are applicable across a range of floodplains from simple to complex.

5.3. Floodplain Channels Are Extensive, Dynamic Networks of Intermittent Streams, but Their Functions Have Not Been Studied

Ephemeral or intermittent channels are hot spots of ecologic and hydrologic change and transformation (e.g., Datry et al., 2017). The floodplain channels described in this study are also intermittent but have so far not been extensively studied. We expect that the eco-hydrologic functions observed in intermittent headwater channels will also be associated with floodplain channels. In headwater systems, the channels are confined so the length of the intermittent stream relative to the active stream is at most one. Finding intermittent headwater streams is then a time-variable problem as the valley wets and dries (e.g., Godsey & Kirchner, 2014; Jencso et al., 2009; Jensen et al., 2017; Ward et al., 2018). Our study site shows clearly the importance of intermittent streams in low-gradient agricultural settings where the total length of intermittent streams activated (1,050 km; Figure 7d) relative to the river channel (24.4 km) is 43. Thus, given that the length of intermittent channels can be much greater in floodplain systems than headwater systems, we might expect amplified eco-hydrologic functioning in intermittent floodplain channels compared to headwater channels. As a first step toward understanding the functioning of ephemeral floodplain channels, we have focused this study on surface-water connectivity. Future work is needed to assess the biogeochemical, sedimentological, and ecological functioning of ephemeral floodplain channels.

We have demonstrated here yet another way in which rivers are intimately connected to their floodplain. Our work underscores that the river corridor is a landscape unit: The river, its hyporheic zone, riparian zone, and floodplain cannot be considered separately but have functions that arise from connectivity (Harvey & Gooseff, 2015). Many connectivity studies emphasize the role of subsurface exchanges (e.g., see references in Harvey & Gooseff, 2015, and Covino, 2017) but have ignored the role of complex surface connections. Our surface-water connectivity findings echo many concepts from the literature on subsurface connectivity (e.g., see references in Harvey & Gooseff, 2015, and Covino, 2017) including that these systems are highly dynamic in time and that key thresholds in the system exist. Furthermore, we would expect river-floodplain systems with floodplain channels to have higher rates of exchange and longer water residence times (compared to the flow in the river). Flow in floodplain channels likely establishes lateral gradients that drive surface-water/groundwater exchange and hyporheic flow, thus increasing water residence times (Malard et al., 2002). These factors that increase water residence times should enhance denitrification processes by allowing more time for the biogeochemical reaction to occur (Böhlke et al., 2009; Duff & Triska, 2000; Mulholland et al., 2008) and, for this system specifically, would do so over a wide range of flows. At the highest flows, the effect of floodplain channels would be washed out, and we would expect channel orientation to drive river-floodplain exchange (Figure 8c), hyporheic flow, and associated nitrate removal (Boano et al., 2014; Gomez-Velez et al., 2017; Stonedahl et al., 2013).

It is unknown how these floodplain channels will morphologically evolve in the future and/or if they represent a transitional floodplain morphology. It is unclear under what hydrologic and sedimentologic conditions a river-floodplain system will (1) remain static, (2) anneal by filling in floodplain channels through sediment deposition (Toonen et al., 2012), (3) avulse by enlarging certain floodplain channels, or (4) evolve to a multichanneled anabranching system (transition from type B3 to C2 floodplain in Nanson & Croke, 1992). The ubiquity and prominence of the floodplain channels along the East Fork White River suggests

they are not filling in with sediment. Velocities in floodplain channels progressively increased with increasing flow, and velocities were highest in the largest, low-lying floodplain channels (Figure 4b). Given that velocity is directly related to shear stress, if these channels are incising, then the largest, low-lying floodplain channels may be incising most rapidly and thus may potentially serve as preferential avulsion pathways. While not a major focus here, our simulations showed the mechanistic precursors for possible channel avulsion, which are not very different mechanistically from those of chute channel cutoff (Harrison et al., 2015). Specifically, where the river channel was oriented transverse to the direction of floodplain flow, at high flows, velocities in the river channel were lower than on the adjacent floodplain (Figure 4b), commensurate with a reduction in flow in the river channel (Figure 5c). This creates the potential for sedimentation in the river channel, further steering flow and potential erosion onto the adjacent floodplain, which could cause the river to avulse into a floodplain channel.

Finally, our findings and the potential benefits of floodplain channels to ecosystem services and functions suggest that floodplains should be managed as part of a comprehensive river corridor strategy. Most current strategies focus solely on flood water storage. The complexity of how these channels evolve, alter residence times, and so forth suggests that floodplains may be important locations for many other processes and should be treated as such. One major implication of floodplain channels in the East Fork White River and floodplain is that this system may serve as a template for restoring/engineering floodplains to reduce nitrate concentrations and loads at moderate and high flows when the majority of nitrate is exported from watersheds. Perhaps in addition to restoring floodplains by simply removing engineered levees (Opperman et al., 2009; Tockner & Stanford, 2002), restoration should also involve altering the floodplain itself to increase connectivity (Kondolf et al., 2006) and improve water quality such as through the creation or enhancement of floodplain channels (Tockner et al., 1999). However, it still remains to be seen how the flow in floodplain channels affects residence times, local groundwater levels, hyporheic exchange, and denitrification processes compared to floodplains without floodplain channels.

6. Summary

We investigated how floodplain channels affect lateral surface-water connectivity between a river and floodplain in a low-gradient river system as a function of flow stage, with a focus on one of the more dramatic examples of a floodplain channel network along the meandering East Fork White River near Seymour, Indiana, USA. Our results highlight that bankfull flow is an oversimplified concept for explaining river-floodplain connectivity because the first major low-lying floodplain channels were inundated roughly 19 days per year. We proposed a conceptual model of river-floodplain connectivity dynamics where the floodplain is activated across a gradient of flows. From this we classify low-gradient, meandering river-floodplain systems as having three distinct flow-dependent regimes: single thread, multithread (occurring roughly 5% of the time for the study reach), and fully inundated (occurring roughly 0.4% of the time). The boundaries of these regimes are fuzzy because when transitioning from the single-thread to the multithread regime, inundated areas may not be well connected to effectively convey flow. Additionally, because when transitioning from the multithread to the fully inundated regime, there may not always be complete inundation of the floodplain as ever higher floodplain channels become inundated creating new floodplain islands. Furthermore, we developed metrics to analyze quantitatively complex river-floodplain systems that include flow in the river channel, bank overtopping, floodplain-island statistics, length of flow paths, correlation between river-floodplain exchange and both bank height and channel orientation, floodplain residence time, and river-floodplain exchange. We envision that these metrics will be useful for comparing various floodplains and as a way to upscale river-floodplain processes (via characterization of exchange and residence time).

Notation

B	index of bank
c	denotes river channel
$d^B_{j;j+1}$	distance along bank B between bank points j and $j+1$ [L]
D^B	total length along bank B [L]

ex denotes exchange
f denotes floodplain
h_m^ξ water depth at grid location m and flow ξ [L]
i index of link in flow path network
j index of bank point
ℓ_i length of link i in the flow path network [L]
ℓ_ξ total length of newly activated flow paths at a given flow ξ [L]
L denotes left bank, oriented downstream
L_ξ total cumulative length of all flow paths that have been activated at or below a given flow ξ [L]
m index of grid location
n number of values statistically analyzed
q_c^ξ average streamwise flux per unit width (or streamwise unit flux) in the river channel at flow ξ [L^2 T^{-1}]
$q_{ex}^{\xi,B}$ average lateral exchange across bank B at flow ξ [L^2 T^{-1}]
$\widetilde{q}_{ex}^{\xi}$ (normalized) river-floodplain exchange at flow ξ
$q_j^{\xi,B}$ lateral flux per unit width (or lateral unit flux) at bank point j across bank B at flow ξ [L^2 T^{-1}]
$\widetilde{q}_j^{\xi,B}$ normalized, smoothed lateral unit flux at bank point j across bank B at flow ξ
$\boldsymbol{q}_m^\xi$ vector of 2-D specific discharge at grid location m and flow ξ [L^2 T^{-1}]
R denotes right bank, oriented downstream
t_c^ξ residence time per unit length in the river channel at flow ξ [T]
t_f^ξ residence time per unit length in the floodplain at flow ξ [T]
$\widetilde{t}_f^{\xi}$ (normalized) floodplain residence time at flow ξ
v_c^ξ average velocity in the river channel at flow ξ [LT^{-1}]
v_f^ξ average velocity in the floodplain at flow ξ [LT^{-1}]
v_i^ξ velocity in link i of the flow path network at flow ξ [LT^{-1}]
$\boldsymbol{v}_m^\xi$ vector of 2-D velocity at grid location m and flow ξ [LT^{-1}]
ξ index of flow
ξ_i index of flow at which link i in the flow path network becomes activated

Acknowledgments
This research was funded in part by the Malcolm and Sylvia Boyce endowment made to Indiana University. J. A. C. was partially supported by the Virginia Agricultural Experiment Station and USDA Hatch program (accession number: 1017457). D. A. E. acknowledges partial support from the donors of the American Chemical Society Petroleum Research fund and IU Grand Challenges *Preparing for Change* initiative for supporting this work. A. S. W. was supported by National Science Foundation awards 1331906 and 1652293. We thank Editor Ilja van Meerveld, the associate editor (anonymous), and three anonymous reviewers for insightful comments that improved the focus and presentation of this manuscript. References to where the data used in this study can be obtained are listed in the main text.

References

Amoros, C., & Bornette, G. (2002). Connectivity and biocomplexity in waterbodies of riverine floodplains. *Freshwater Biology*, *47*(4), 761–776. https://doi.org/10.1046/j.1365-2427.2002.00905.x

Benke, A. C., Chaubey, I., Ward, G. M., & Dunn, E. L. (2000). Flood pulse dynamics of an unregulated river floodplain in the southeastern U.S. coastal plain. *Ecology*, *81*(10), 2730–2741. https://doi.org/10.1890/0012-9658(2000)081[2730:FPDOAU]2.0.CO;2

Boano, F., Harvey, J. W., Marion, A., Packman, A. I., Revelli, R., Ridolfi, L., & Wörman, A. (2014). Hyporheic flow and transport processes: Mechanisms, models, and biogeochemical implications. *Reviews of Geophysics*, *52*, 603–679. https://doi.org/10.1002/2012RG000417

Bogoni, M., Putti, M., & Lanzoni, S. (2017). Modeling meander morphodynamics over self-formed heterogeneous floodplains. *Water Resources Research*, *53*, 5137–5157. https://doi.org/10.1002/2017WR020726

Böhlke, J. K., Antweiler, R. C., Harvey, J. W., Laursen, A. E., Smith, L. K., Smith, R. L., & Voytek, M. A. (2009). Multi-scale measurements and modeling of denitrification in streams with varying flow and nitrate concentration in the upper Mississippi River basin, USA. *Biogeochemistry*, *93*(1–2), 117–141. https://doi.org/10.1007/s10533-008-9282-8

Bracken, L. J., Wainwright, J., Ali, G. A., Tetzlaff, D., Smith, M. W., Reaney, S. M., & Roy, A. G. (2013). Concepts of hydrological connectivity: Research approaches, pathways and future agendas. *Earth-Science Reviews*, *119*, 17–34. https://doi.org/10.1016/j.earscirev.2013.02.001

Brice, J. C. (1974). Evolution of meander loops. *GSA Bulletin*, *85*(4), 581–586. https://doi.org/10.1130/0016-7606(1974)85<581:EOML>2.0.CO;2

Brunner, G. W. (2016). *HEC-RAS river analysis system, 2D modeling user's manual version 5.0. (Rep. CPD-68A)*. Davis, CA: U.S. Army Corps of Engineers.

Bryant-Mason, A., Xu, Y. J., & Altabet, M. A. (2013). Limited capacity of river corridor wetlands to remove nitrate: A case study on the Atchafalaya River Basin during the 2011 Mississippi River flooding. *Water Resources Research*, *49*, 283–290. https://doi.org/10.1029/2012WR012185

Camporeale, C., Perona, P., Porporato, A., & Ridolfi, L. (2005). On the long-term behavior of meandering rivers. *Water Resources Research*, *41*, W12403. https://doi.org/10.1029/2005WR004109

Casulli, V. (2009). A high-resolution wetting and drying algorithm for free-surface hydrodynamics. *International Journal for Numerical Methods in Fluids*, *60*(4), 391–408. https://doi.org/10.1002/fld.1896

Covino, T. (2017). Hydrologic connectivity as a framework for understanding biogeochemical flux through watersheds and along fluvial networks. *Geomorphology*, *277*, 133–144. https://doi.org/10.1016/j.geomorph.2016.09.030

Crawford, C. G., Lydy, M. J., & Frey, J. W. (1996). Fishes of the White River Basin, Indiana. *U.S. Geological Survey Water-Resources Investigations Report 96–4232*, 8 P. Reston, VA: U.S. Geological Survey.

Datry, T., Bonada, N., & Boulton, A. (2017). *Intermittent rivers and ephemeral streams: Ecology and management* (p. 622). San Diego, CA: Academic.

David, S. R., Czuba, J. A., & Edmonds, D. A. (2018). Channelization of meandering river floodplains by headcutting. *Geology*, *47*(1), 15–18. https://doi.org/10.1130/G45529.1

David, S. R., Edmonds, D. A., & Letsinger, S. L. (2017). Controls on the occurrence and prevalence of floodplain channels in meandering rivers. *Earth Surface Processes and Landforms*, *42*(3), 460–472. https://doi.org/10.1002/esp.4002

Duff, J. H., & Triska, F. J. (2000). Nitrogen biogeochemistry and surface-subsurface exchange in streams. In J. B. Jones & P. J. Mulholland (Eds.), *Streams and Ground Waters* (pp. 197–220). San Diego, CA: Academic. https://doi.org/10.1016/B978-012389845-6/50009-0

Eke, E., Parker, G., & Shimizu, Y. (2014). Numerical modeling of erosional and depositional bank processes in migrating river bends with self-formed width: Morphodynamics of bar push and bank pull. *Journal of Geophysical Research: Earth Surface*, *119*, 1455–1483. https://doi.org/10.1002/2013JF003020

Fagan, S. D., & Nanson, G. C. (2004). The morphology and formation of floodplain-surface channels, Cooper Creek, Australia. *Geomorphology*, *60*(1-2), 107–126. https://doi.org/10.1016/j.geomorph.2003.07.009

Findlay, S. (1995). Importance of surface-subsurface exchange in stream ecosystems: The hyporheic zone. *Limnology and Oceanography*, *40*(1), 159–164. https://doi.org/10.4319/lo.1995.40.1.0159

Fisk, H. N. (1944). *Geological investigation of the Alluvial Valley of the Lower Mississippi River*. Vicksburg, MS: U.S. Army Corps of Engineers.

Fisk, H. N. (1947). Fine-grained alluvial deposits and their effect on Mississippi River activity. (Rep. MRC-WES-2000-2-48). Vicksburg, MS: Waterways Experiment Station, U.S. Army Corps of Engineers.

Forshay, K. J., & Stanley, E. H. (2005). Rapid nitrate loss and denitrification in a temperate river floodplain. *Biogeochemistry*, *75*(1), 43–64. https://doi.org/10.1007/s10533-004-6016-4

Freeman, M. C., Pringle, C. M., & Jackson, C. R. (2007). Hydrologic connectivity and the contribution of stream headwaters to ecological integrity at regional scales. *Journal of the American Water Resources Association*, *43*(1), 5–14. https://doi.org/10.1111/j.1752-1688.2007.00002.x

Godsey, S. E., & Kirchner, J. W. (2014). Dynamic, discontinuous stream networks: Hydrologically driven variations in active drainage density, flowing channels and stream order. *Hydrological Processes*, *28*(23), 5791–5803. https://doi.org/10.1002/hyp.10310

Gomez-Velez, J. D., Wilson, J. W., Cardenas, M. B., & Harvey, J. W. (2017). Flow and residence times of dynamic river bank storage and sinuosity-driven hyporheic exchange. *Water Resources Research*, *53*, 8572–8595. https://doi.org/10.1002/2017WR021362

Harrison, L. R., Dunne, T., & Fisher, G. B. (2015). Hydraulic and geomorphic processes in an overbank flood along a meandering, gravel-bed river: Implications for chute formation. *Earth Surface Processes and Landforms*, *40*(9), 1239–1253. https://doi.org/10.1002/esp.3717

Harvey, J., & Gooseff, M. (2015). River corridor science: Hydrologic exchange and ecological consequences from bedforms to basins. *Water Resources Research*, *51*, 6893–6922. https://doi.org/10.1002/2015WR017617

Hasegawa, K. (1977). Computer simulation of the gradual migration of meandering channels. In *Proceedings of the Hokkaido Branch*, (pp. 197–202). Jpn. Soc. of Civ. Eng.

Homer, C. G., Dewitz, J. A., Yang, L., Jin, S., Danielson, P., Xian, G., et al. (2015). Completion of the 2011 National Land Cover Database for the conterminous United States—Representing a decade of land cover change information. *Photogrammetric Engineering and Remote Sensing*, *81*(5), 345–354.

Howard, A. D. (1992). Modelling channel migration and floodplain development in meandering streams. In P. A. Carling & G. E. Petts (Eds.), *Lowland Floodplain Rivers: Geomorphological Perspectives* (pp. 1–42). Chichester, UK: Wiley.

Howard, A. D. (1996). Modelling channel evolution and floodplain morphology. In M. G. Anderson, P. D. Bates, & D. E. Walling (Eds.), *Floodplain Processes* (pp. 15–62). Hoboken, NJ: Wiley.

Howard, A. D., & Knutson, T. R. (1984). Sufficient conditions for river meandering: A simulation approach. *Water Resources Research*, *20*, 1659–1667. https://doi.org/10.1029/WR020i011p01659

Ikeda, S., Parker, G., & Sawai, K. (1981). Bend theory of river meanders. Part 1. Linear development. *Journal of Fluid Mechanics*, *112*, 363–377. https://doi.org/10.1017/S0022112081000451

Interagency Committee on Water Data (IACWD) (1982). Guidelines for determining flood flow frequency: Bulletin 17B of the Hydrological Subcommittee: Washington, D.C., U.S. Geological Survey Office of Water Data Coordination.

James, C. S. (1985). Sediment transfer to overbank sections. *Journal of Hydraulic Research*, *23*(5), 435–452. https://doi.org/10.1080/00221688509499337

Jencso, K. G., McGlynn, B. L., Gooseff, M. N., Wondzell, S. M., Bencala, K. E., & Marshall, L. A. (2009). Hydrologic connectivity between landscapes and streams: Transferring reach- and plot-scale understanding to the catchment scale. *Water Resources Research*, *45*, W04428. https://doi.org/10.1029/2008WR007225

Jensen, C. K., McGuire, K. J., & Prince, P. S. (2017). Headwater stream length dynamics across four physiographic provinces of the Appalachian highlands. *Hydrological Processes*, *31*(19), 3350–3363. https://doi.org/10.1002/hyp.11259

Johannesson, H., & Parker, G. (1989). Linear theory of river meanders. In S. Ikeda & G. Parker (Eds.), *River Meandering* (pp. 181–213). Washington, DC: American Geophysical Union. https://doi.org/10.1029/WM012p0181

Junk, W., Bayley, P., & Sparks, R. (1989). The flood pulse concept in river-floodplain systems. *Canadian Special Publication on Fisheries and Aquatic Sciences*, *106*, 110–127.

Knight, D., & Shiono, K. (1996). River channel and floodplain hydraulics. In M. G. Anderson, P. D. Bates, & D. E. Walling (Eds.), *Floodplain Processes* (pp. 139–182). Hoboken, NJ: Wiley.

Kondolf, G. M., Boulton, A. J., O'Daniel, S., Poole, G. C., Rahel, F. J., Stanley, E. H., et al. (2006). Process-based ecological river restoration: Visualizing three-dimensional connectivity and dynamic vectors to recover lost linkages. *Ecology and Society*, *11*(2), 5. http://www.ecologyandsociety.org/vol11/iss2/art5/

Kupfer, J. A., Meitzen, K. M., & Gao, P. (2015). Flooding and surface connectivity of *Taxodium-Nyssa* stands in a southern floodplain forest ecosystem. *River Research and Applications*, *31*(10), 1299–1310. https://doi.org/10.1002/rra.2828

Lauer, J. W., & Parker, G. (2008). Modeling framework for sediment deposition, storage, and evacuation in the floodplain of a meandering river: Theory. *Water Resources Research*, *44*, W04425. https://doi.org/10.1029/2006WR005528

Lauer, J. W., & Willenbring, J. (2010). Steady state reach-scale theory for radioactive tracer concentration in a simple channel/floodplain system. *Journal of Geophysical Research*, *115*, F04018. https://doi.org/10.1029/2009JF001480

Leopold, L. B., Wolman, M. G., & Miller, J. P. (1964). *Fluvial processes in geomorphology*. San Francisco, CA: W. H. Freeman and Company.

Lewin, J., & Ashworth, P. J. (2014). The negative relief of large river floodplains. *Earth-Science Reviews*, *129*, 1–23. https://doi.org/10.1016/j.earscirev.2013.10.014

Lewin, J., Ashworth, P. J., & Strick, R. J. P. (2017). Spillage sedimentation on large river floodplains. *Earth Surface Processes and Landforms*, *42*(2), 290–305. https://doi.org/10.1002/esp.3996

Limaye, A. B. (2017). Extraction of multithread channel networks with a reduced-complexity flow model. *Journal of Geophysical Research: Earth Surface*, *122*, 1972. https://doi.org/10.1002/2016JF004175–1990.

Mackin, J. H. (1937). Erosional history of the Big Horn Basin, Wyoming. *Geological Society of America Bulletin*, *48*(6), 813–894. https://doi.org/10.1130/GSAB-48-813

Malard, F., Tockner, K., Dole-Oliver, M.-J., & Ward, J. V. (2002). A landscape perspective of surface-subsurface hydrological exchanges in river corridors. *Freshwater Biology*, *47*(4), 621–640. https://doi.org/10.1046/j.1365-2427.2002.00906.x

Mertes, L. A., Dunne, T., & Martinelli, L. A. (1996). Channel-floodplain geomorphology along the Solimões-Amazon River, Brazil. *Geological Society of America Bulletin*, *108*(9), 1089–1107. https://doi.org/10.1130/0016-7606(1996)108<1089:CFGATS>2.3.CO;2

Mertes, L. A. K. (1997). Documentation and significance of the perirheic zone on inundated floodplains. *Water Resources Research*, *33*, 1749–1762. https://doi.org/10.1029/97WR00658

Morlock, S. E., Menke, C. D., Arvin, D. V., & Kim, M. H. (2008). Flood of June 7–9, 2008, in central and southern Indiana. *U.S. Geological Survey Open File Report 2008–1322*, 15 p., 3 app. Reston, VA: U.S. Geological Survey. https://pubs.usgs.gov/of/2008/1322/

Motta, D., Abad, J. D., Langendoen, E. J., & García, M. H. (2012a). A simplified 2D model for meander migration with physically-based bank evolution. *Geomorphology*, *163-164*, 10–25. https://doi.org/10.1016/j.geomorph.2011.06.036

Motta, D., Abad, J. D., Langendoen, E. J., & García, M. H. (2012b). The effects of floodplain soil heterogeneity on meander planform shape. *Water Resources Research*, *48*, W09518. https://doi.org/10.1029/2011WR011601

Mueller, D. S., & Wagner, C. R. (2009). Measuring discharge with acoustic Doppler current profilers from a moving boat. *U.S. Geol. Surv. Tech. Meth., 3A-22*, 72 P. Reston, VA: U.S. Geological Survey. http://pubs.water.usgs.gov/tm3a22

Mulholland, P. J., Helton, A. M., Poole, G. C., Hall, R. O., Hamilton, S. K., Peterson, B. J., et al. (2008). Stream denitrification across biomes and its response to anthropogenic nitrate loading. *Nature*, *452*(7184), 202–205. https://doi.org/10.1038/nature06686.

Nanson, G. C., & Croke, J. C. (1992). A genetic classification of floodplains. *Geomorphology*, *4*(6), 459–486. https://doi.org/10.1016/0169-555X(92)90039-Q

Nicholas, A. P., Walling, D. E., Sweet, R. J., & Fang, X. (2006). Development and evaluation of a new catchment-scale model of floodplain sedimentation. *Water Resources Research*, *42*, W10426. https://doi.org/10.1029/2005WR004579

Odgaard, A. J. (1989a). River-meander model. I: Development. *Journal of Hydraulic Engineering*, *115*(11), 1433–1450. https://doi.org/10.1061/(ASCE)0733-9429(1989)115:11(1433)

Odgaard, A. J. (1989b). River-meander model. II: Applications. *Journal of Hydraulic Engineering*, *115*(11), 1451–1464. https://doi.org/10.1061/(ASCE)0733-9429(1989)115:11(1451)

OpenTopography (2013). Indiana 2011–2013 statewide lidar data available. La Jolla, CA: Univ. of California San Diego. http://www.opentopography.org/news/indiana-2011-2013-statewide-lidar-survey-data-available

Opperman, J. J., Galloway, G. E., Fargione, J., Mount, J. F., Richter, B. D., & Secchi, S. (2009). Sustainable floodplains through large-scale reconnection to rivers. *Science*, *326*(5959), 1487–1488. https://doi.org/10.1126/science.1178256

Park, E., & Latrubesse, E. M. (2017). The hydro-geomorphologic complexity of the lower Amazon River floodplain and hydrological connectivity assessed by remote sensing and field control. *Remote Sensing of Environment*, *198*, 321–332. https://doi.org/10.1016/j.rse.2017.06.021

Parsons, D. R., Jackson, P. R., Czuba, J. A., Engel, F. L., Rhoads, B. L., Oberg, K. A., et al. (2013). Velocity Mapping Toolbox (VMT): A processing and visualization suite for moving-vessel ADCP measurements. *Earth Surface Processes and Landforms*, *38*(11), 1244–1260. https://doi.org/10.1002/esp.3367

Pizzuto, J. E. (1987). Sediment diffusion during overbank flows. *Sedimentology*, *34*(2), 301–317. https://doi.org/10.1111/j.1365-3091.1987.tb00779.x

Rak, G., Kozelj, D., & Steinman, F. (2016). The impact of floodplain land use on flood wave propagation. *Natural Hazards*, *83*(1), 425–443. https://doi.org/10.1007/s11069-016-2322-0

Robinson, B.A. (2013). Regional bankfull-channel dimensions of non-urban wadeable streams in Indiana. *U.S. Geological Survey Scientific Investigations Report 2013–5078*, 33 p. Reston, VA: U.S. Geological Survey. http://pubs.usgs.gov/sir/2013/5078

Schwenk, J., Lanzoni, S., & Foufoula-Georgiou, E. (2015). The life of a meander bend: Connecting shape and dynamics via analysis of a numerical model. *Journal of Geophysical Research: Earth Surface*, *120*, 690–710. https://doi.org/10.1002/2014JF003252

Seminara, G. (2006). Meanders. *Journal of Fluid Mechanics*, *554*(1), 271–297. https://doi.org/10.1017/S0022112006008925

Stonedahl, S. H., Harvey, J. W., & Packman, A. I. (2013). Interactions between hyporheic flow produced by stream meanders, bars, and dunes. *Water Resources Research*, *49*, 5450–5461. https://doi.org/10.1002/wrcr.20400

Sturm, T. W. (2001). *Open channel hydraulics*. New York, NY: McGraw-Hill.

Sun, T., Meakin, P., & Jøssang, T. (2001a). A computer model for meandering rivers with multiple bed load sediment sizes: 1. Theory. *Water Resources Research*, *37*, 2227–2241. https://doi.org/10.1029/2000WR900396

Sun, T., Meakin, P., & Jøssang, T. (2001b). A computer model for meandering rivers with multiple bed load sediment sizes: 2. Computer simulations. *Water Resources Research*, *37*, 2243–2258. https://doi.org/10.1029/2000WR900397

Sun, T., Meakin, P., & Jøssang, T. (2001c). Meander migration and the lateral tilting of floodplains. *Water Resources Research*, *37*, 1485–1502. https://doi.org/10.1029/2000WR900343

Sun, T., Meakin, P., Jøssang, T., & Schwarz, K. (1996). A simulation model for meandering rivers. *Water Resources Research*, *32*, 2937–2954. https://doi.org/10.1029/96WR00998

Tockner, K., Pennetzdorfer, D., Reiner, N., Schiemer, F., & Ward, J. V. (1999). Hydrological connectivity, and the exchange of organic matter and nutrients in a dynamic river-floodplain system (Danube, Austria). *Freshwater Biology*, *41*(3), 521–535. https://doi.org/10.1046/j.1365-2427.1999.00399.x

Tockner, K., & Stanford, J. A. (2002). Riverine flood plains: Present state and future trends. *Environmental Conservation*, *29*(03), 308–330. https://doi.org/10.1017/S037689290200022X

Toonen, W. H. J., Kleinhans, M. G., & Cohen, K. M. (2012). Sedimentary architecture of abandoned channel fills. *Earth Surface Processes and Landforms*, *37*(4), 459–472. https://doi.org/10.1002/esp.3189

Trigg, M. A., Bates, P. D., Wilson, M. D., Schumann, G., & Baugh, C. (2012). Floodplain channel morphology and networks of the middle Amazon River. *Water Resources Research*, *48*, W10504. https://doi.org/10.1029/2012WR011888

U.S. Geological Survey (USGS) (2016). WaterWatch: Customized rating curve builder for site 03365500. Reston, VA: U.S. Geological Survey. (last accessed 17 Nov. 2016) https://waterwatch.usgs.gov
U.S. Geological Survey (USGS) (2017). USGS 03365500 East Fork White River at Seymour, IN. Reston, VA: U.S. Geological Survey. (last accessed 10 Oct. 2017) https://waterdata.usgs.gov/nwis/inventory/?site_no=03365500&agency_cd=USGS
van Dijk, W. M., Teske, R., van de Lageweg, W. I., & Kleinhans, M. G. (2013). Effects of vegetation distribution on experimental river channel dynamics. *Water Resources Research*, *49*, 7558–7574. https://doi.org/10.1002/2013WR013574
van Dijk, W. M., van de Lageweg, W. I., & Kleinhans, M. G. (2012). Experimental meandering river with chute cutoffs. *Journal of Geophysical Research*, *117*, F03023. https://doi.org/10.1029/2011JF002314
van Dijk, W. M., van de Lageweg, W. I., & Kleinhans, M. G. (2013). Formation of a cohesive floodplain in a dynamic experimental meandering river. *Earth Surface Processes and Landforms*, *38*(13), 1550–1565. https://doi.org/10.1002/esp.3400
Viparelli, E., Lauer, J. W., Belmont, P., & Parker, G. (2013). A numerical model to develop long-term sediment budgets using isotopic sediment fingerprints. *Computers & Geosciences*, *53*, 114–122. https://doi.org/10.1016/j.cageo.2011.10.003
Ward, A. S., Schmadel, N. M., & Wondzell, S. M. (2018). Simulation of dynamic expansion, contraction, and connectivity in a mountain stream network. *Advances in Water Resources*, *114*, 64–82. https://doi.org/10.1016/j.advwatres.2018.01.018
Ward, J. V., & Stanford, J. A. (1995). The serial discontinuity concept: Extending the model to floodplain rivers. *Regulated Rivers: Research and Management*, *10*(2–4), 159–168. https://doi.org/10.1002/rrr.3450100211
Williams, G. P. (1978). Bank-full discharge of rivers. *Water Resources Research*, *14*, 1141–1154. https://doi.org/10.1029/WR014i006p01141
Wolman, M. G., & Leopold, L. B. (1957). River flood plains: Some observations on their formation, *U.S. Geological Survey Professional Paper, 282-C*, 87–107. Reston, VA: U.S. Geological Survey.

Erratum

In the originally published version of this article, there was an error in the text: In section 3.3, the text in the seventh sentence of the fifth paragraph should read “MAE of 0.21.” The error has since been corrected, and this version may be considered the authoritative version of record.